https://doi.org/10.5194/wes-2026-93
Preprint. Discussion started: 29 June 2026


eawe european academy of wind energy
Open Access WIND ENERGY SCIENCE DISCUSSIONS

# On the effects of wind shear and veer on the power of a downstream turbine

Carlo R. Sucameli[1], Marta Bertelè[2], Robert Braunbehrens[1], Filippo Campagnolo[1], Simone Tamaro[1], Paul Hulsman[3, 4], and Carlo L. Bottasso[1]

[1]Wind Energy Institute, Technische Universität München, Garching bei München, 85748 Germany
[2]Siemens Gamesa Renewable Energy, Beim Strohhause 17–31, 20097 Hamburg, Germany
[3]Carl von Ossietzky Universität Oldenburg, School of Mathematics and Natural Sciences, Institute of Physics, Oldenburg, 26129, Niedersachsen, Germany
[4]ForWind – Center for Wind Energy Research, Küpkersweg 70, Oldenburg, 26129, Niedersachsen, Germany

**Correspondence:** Carlo L. Bottasso (carlo.bottasso@tum.de)

**Abstract.**

Understanding flow behavior within wind farms remains one of the central challenges in wind energy research, where wakes play a prominent role by coupling individual machines together. In fact, turbines are frequently operated under waked conditions, with wake effects on power production further modulated by atmospheric stability at the site. This paper investigates the influence of wind shear and veer on the power output of a waked wind turbine. The analysis is based on field measurements from two aligned wind turbines operating under inflow conditions that are often strongly sheared and veered. The results demonstrate that both shear and veer significantly affect wake characteristics and trajectory. Because isolating their individual contributions from field data alone is challenging, dedicated computational fluid dynamics (CFD) simulations were performed, confirming the experimental observations and enabling the effects of shear and veer to be disentangled.

The performance of several wake models was evaluated against experimental data, showing that prediction accuracy can be improved by explicitly accounting for shear and veer effects. This improved accuracy could be leveraged to support various applications. To explore the potential benefits in one exemplary use case, we consider shear- and veer-enhanced models in the context of wake-steering wind farm control. This application, however, requires real-time estimates of wind gradients, which are not available from standard onboard anemometry. To overcome this limitation, a wind sensing technique based on blade load measurements is employed to estimate shear and veer during operation. Furthermore, the strong correlation between these two quantities observed at the test site is exploited to simplify practical implementation. Wake-steering simulations indicate that incorporating shear and veer into the control strategy can lead to improved power capture.

## 1 Introduction

The expansion of the wind energy sector over recent years has driven a rapid reduction in the levelized cost of energy (LCOE), a trend that is expected to continue (Wiser et al., 2021). The pursuit of lower electricity generation costs has led to the deployment of increasingly large wind farms, in which turbines are clustered together to exploit advantages in land use, shared

https://doi.org/10.5194/wes-2026-93
Preprint. Discussion started: 29 June 2026


eawe european academy of wind energy
Open Access WIND ENERGY SCIENCE DISCUSSIONS

infrastructure, and coordinated operation and maintenance. As a result, wind energy research is progressively shifting its focus from the individual turbine level toward an integrated wind farm perspective.

Wind farm flows are complex phenomena that remain the subject of active research and represent one of the key challenges to the broader deployment of wind energy (Meyers et al., 2022). Their characteristics are tightly linked to the ones of the atmospheric boundary layer (ABL) at a given site, and are influenced by terrain orography, vegetation, and obstacles, as well as by atmospheric stability. Stability conditions are further modulated by temporal patterns acting across multiple time scales (e.g., diurnal and seasonal). These stability characteristics drive the formation of wind gradients, such as vertical wind shear and horizontal directional veer (Stoevesandt et al., 2020), which can significantly affect the operation of wind turbines and the evolution of the wakes that develop behind their rotors.

This paper considers the effects of wind shear and veer on wakes at three different levels: first we try to improve the understanding of the underlying physics; next, we leverage this understanding to improve models of wakes; and, finally, we leverage the improved models to improve performance in a relevant exemplary application. Sharper physical insight and better models support the continued development of wind energy technologies and products. Specifically, enhanced modeling capabilities can enable better wind turbine and wind farm designs, their improved operation, and more accurate energy yield and consumed lifetime estimations. To exemplify the potential benefits, here we apply a shear- and veer-aware model to wake-steering wind farm control, an application where the accuracy of wake models plays a central role. The work at these three levels is guided in this paper by three main scientific questions.

The first scientific question addressed here is: *"What is the impact of wind shear and veer on the power produced by a waked wind turbine?"*

Both wind shear and veer are complex inflow characteristics that vary with atmospheric stratification and are governed by surface friction and Coriolis forces. A substantial body of field-based research has confirmed that these two quantities can significantly affect the power production of modern wind turbines (Wharton and Lundquist, 2012; Vanderwende and Lundquist, 2012; Sanchez Gomez and Lundquist, 2020). These effects are observed not only for waked turbines but also for turbines operating in free-stream conditions, as shown in Bulaevskaya et al. (2015) and Howland et al. (2020). The influence of atmospheric stability on wake development has been investigated using large-eddy simulations (LES) (Vollmer et al., 2016; Abkar and Porté-Agel, 2015), numerical modeling (Bromm et al., 2017; Churchfield and Sirnivas, 2018), and field measurements (Bodini et al., 2017). These studies revealed that veered inflows induce wakes whose cross sections stretch into ellipsoidal shapes. Furthermore, Englberger and Lundquist (2020); Englberger et al. (2020) numerically investigated wake evolution under veered inflow conditions, showing that stronger veer can accelerate wake recovery. Shu et al. (2020) showed that veer can be influenced by terrain complexity, and that its impact on the power production of utility-scale wind turbines depends on the specific veer profile across the rotor (Gao et al., 2021, 2024).

The present paper uses an experimental dataset to evaluate the impact of wind shear and veer on the wake generated by an upstream turbine, focusing on the resulting effects on the power producted by a downstream turbine. A dedicated measurement campaign was conducted by eno energy systems, TUM, and ForWind on two 3.5 MW wind turbines. For the purposes of this study, approximately one year of high-quality measurements – including met-mast data, SCADA data, and blade load

https://doi.org/10.5194/wes-2026-93
Preprint. Discussion started: 29 June 2026


eawe european academy of wind energy
Open Access WIND ENERGY SCIENCE DISCUSSIONS

measurements – was collected from the non-misaligned turbines and analyzed. A distinctive feature of the test site is the frequent occurrence of strong vertical wind shear and pronounced wind direction veer. As demonstrated in this paper, both quantities have a measurable influence on the power production of the downstream turbine.

Due to the natural interdependence between wind shear and veer, isolating the individual impact of each quantity is challenging in field measurements. To obtain a more phenomenological understanding of the underlying mechanisms, and to avoid biases introduced by other effects such as complex terrain, a set of high-fidelity large-eddy simulations is performed in which only wind shear is varied. The simulations confirm the trends observed in the field, showing that increasing wind shear leads to a progressively larger lateral displacement of the wake toward the right when viewed in the downstream direction. Using a recent model developed at TUM (Tamaro et al., 2024), this behavior can be at least partially explained by the presence of a non-zero residual lateral force acting on the rotor, which is proportional to wind shear.

This naturally leads to the second research focus of the paper, which is closely related to wind farm modeling and control and addresses the question: *"Can wind farm model predictions be improved by explicitly accounting for the effects of wind shear and veer?"*

In recent years, a wide range of wake models with increasing levels of sophistication has been developed to represent the complexity of turbine-to-turbine interactions in wind farms. These range from fast steady-state engineering models (Bastankhah and Porté-Agel, 2014; Abkar and Porté-Agel, 2015; Blondel and Cathelain, 2020; FLORIS, 2025) and their dynamic extensions (Becker et al., 2022; Braunbehrens et al., 2022), to mid-fidelity approaches (Jonkman and Shaler, 2021), all the way to high-fidelity computational fluid dynamics (CFD) (Kuhn et al., 2025).

The present work focuses on fast steady-state engineering wake models, which are widely used for energy yield assessment, layout and operational optimization, wind farm control, and other applications requiring large numbers of flow realizations. Despite their relative simplicity, these models can deliver good predictive performance in many cases, particularly when calibrated against high-fidelity simulations (Fleming et al., 2017; Doekemeijer et al., 2021) or field measurements (Howland et al., 2019; Schreiber et al., 2020b; Braunbehrens et al., 2023). However, calibration alone cannot compensate for physical processes that are not explicitly represented in the model formulation. To address this limitation, the present study incorporates the effects of wind shear and veer into an engineering wake model and demonstrates that their inclusion leads to a measurable improvement in predictive accuracy.

Wind farm control is one of the various application areas that can substantially benefit from fast engineering models with improved predictive accuracy (Meyers et al., 2022). Among the various strategies proposed to enhance wind farm power production, wake steering has emerged as one of the most promising and extensively studied approaches (Fleming et al., 2019, 2020). Wake steering exploits the fact that a yaw-misaligned turbine deflects the wake shed by its rotor. By deliberately offsetting the yaw orientation of upstream turbines relative to the incoming wind direction, wake impingement on downstream turbines can be reduced, thereby increasing the overall power production of the wind plant.

Wake steering strategies are typically implemented by prescribing yaw offsets to individual turbine controllers. These offsets are usually computed offline and stored in lookup tables (LUTs) as functions of relevant inflow parameters, such as wind speed, wind direction, and turbulence intensity. Uncertainties in these quantities can also be incorporated during the optimiza-

https://doi.org/10.5194/wes-2026-93
Preprint. Discussion started: 29 June 2026




tion process (Simley et al., 2020; Rott et al., 2018). During operation, the LUTs are interpolated in real time to determine the appropriate inflow-dependent yaw offsets. The computation of these offsets relies on control-oriented engineering flow models, which explicitly account for the effects of yaw misalignment on wake evolution (FLORIS, 2025; Martínez-Tossas et al., 2019, 2021).

As in other applications relying on engineering models, predictive accuracy can be enhanced by incorporating additional relevant physical processes. Engineering wake models are, in fact, evolving rapidly. For example, Gebraad et al. (2016a) and Abkar et al. (2018) proposed modifications to the Gaussian wake model to account for the effects of veered inflow. More recently, Mohammadi et al. (2022) developed an extension of the curled-wake model that explicitly includes inflow veer.

Along these lines, this work demonstrates that explicitly incorporating wind shear and veer into a control-oriented engineering wake model improves its predictive accuracy by capturing their effects on wake displacement and skewing. It is reasonable to expect that such improved modeling accuracy could translate into enhanced performance of a wake-steering controller synthesized from a shear- and veer-aware wake model. While a field-based validation of this concept was not feasible within the scope of the present study, shear- and veer-aware power-boosting wake steering is investigated through simulations. The results indicate that the improved models have the potential to enhance control performance.

However, the idea of including inflow gradients in wind farm control – although appealing for its potential to improve wake modeling accuracy – requires the ability to estimate these quantities during operation. This consideration leads to the third and final question investigated in the present paper: *"How can shear and veer be estimated in the field?"*. In fact, standard wind turbines are generally equipped with onboard anemometry that is unable to resolve wind gradients across the rotor disk.

Here we address this problem by using "the rotor as a sensor" (Kim et al., 2023), a technique that estimates inflow conditions from SCADA data and measured blade loads. Although this method is able to measure both shear and veer (Bertelè et al., 2024), to simplify the implementation, in the present work only vertical shear is estimated from turbine operational data, while veer is inferred from the strong correlation observed between these two quantities at the investigated site.

The paper is organized as follows. Section 2 describes the field experimental campaign. The test site and the main statistics of the measured wind are presented in Sect. 2.1 and Sect. 2.2, respectively, while the effects of wind shear and veer on a downstream turbine are investigated in Sect. 2.3. Section 3 introduces the models adopted in this work, which include a high-fidelity LES model (Sect. 3.1), an analytical model of the shear-induced lateral force responsible for wake displacement (Sect. 3.2 and 3.3), and shear- and veer-aware wake models (Sect. 3.4) that – for control applications – are informed by a wind estimator of the inflow conditions being encountered. Section 4 presents the results, first discussing model tuning and sensitivity in Sects. 4.1 and 4.2, followed by Sects. 4.3 and 4.4 that analyze the accuracy of the different models against field measurements; the potential benefits of the enhanced models for wake-steering control are assessed through numerical simulations in Sect. 4.5. Finally, Sect. 5 summarizes the main findings and key takeaways.

https://doi.org/10.5194/wes-2026-93
Preprint. Discussion started: 29 June 2026


eawe european academy of wind energy
Open Access WIND ENERGY SCIENCE DISCUSSIONS

## 2 Free field experiments

### 2.1 Test site and measurement setup

The test site is located in northern Germany, approximately 10 Km inland from the Baltic Sea, with prevailing southwesterly winds. Two wind turbines that are frequently aligned with the dominant wind direction were selected from a larger cluster to investigate wake effects on the downstream turbine in terms of power production and structural loads. Both turbines have a rated power of 3.5 MW and a rotor diameter of 126 m, with hub heights of 117 m for the upstream turbine (WT1) and 137 m for the downstream turbine (WT2). The inter-turbine spacing is approximately 336 m, corresponding to about 2.7 rotor diameters D.

To enable accurate inflow characterization, a meteorological mast was installed 300 m northwest of WT1. The mast was equipped with wind cup anemometers and wind vanes at approximately hub height and near the lower tip height of WT1. This configuration allows for the estimation of vertical wind shear and directional veer, which cannot be resolved using standard pointwise onboard anemometry. To assess loading conditions under waked and non-waked operation and to support the validation of wind sensing techniques, the blades of both turbines were instrumented with strain gauges at the blade roots. A satellite image of the test site is shown in Fig. 1a. The local wind rose, shown in Fig. 1b, is characterized by a predominance of southwesterly winds, occurring mostly at wind speeds below the rated value of 11.3 $ms^{-1}$ for both turbines.

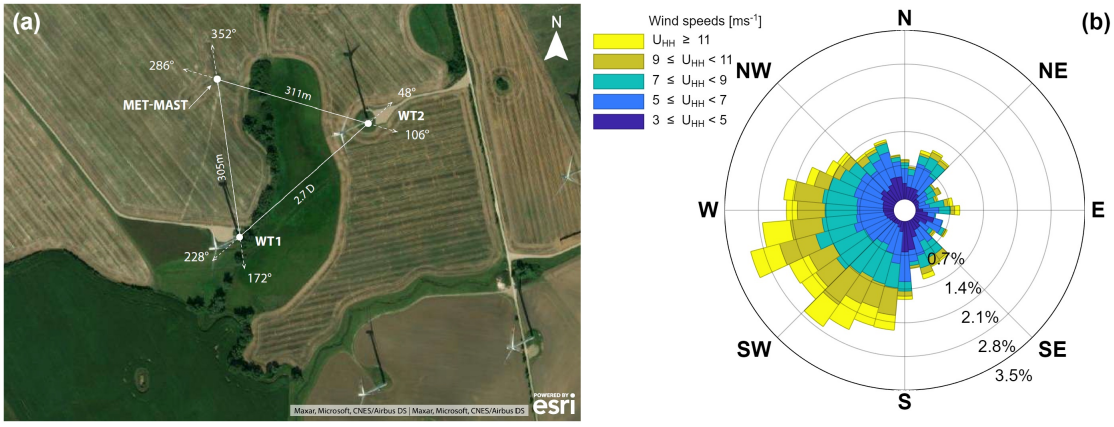


**Figure 1.** Aerial view (© ESRI) **(a)** and wind rose **(b)** of the experimental test site.

During the measurement campaign, 12 months of data were collected between December 2019 and December 2020, including SCADA records, met-mast measurements, and blade load data. All results presented in this paper refer to non-yawed operating conditions; therefore, data corresponding to upstream turbine yaw misalignments exceeding 5° were excluded. The remaining data were aggregated into 10-minute averaged samples. Operating conditions unsuitable for the analysis – such as curtailment, turbine shutdowns, incomplete bins, or sensor unavailability – were also discarded.

https://doi.org/10.5194/wes-2026-93
Preprint. Discussion started: 29 June 2026


eawe european academy of wind energy
Open Access WIND ENERGY SCIENCE DISCUSSIONS

Furthermore, only waked conditions, in which WT1 partially or fully wakes WT2, were considered. This required restricting the wind direction to the range 180°–260°. After applying all filtering criteria, the final dataset comprised 3,378 samples, corresponding to approximately 23 days of continuous measurements.

### 2.2 Analysis of the wind characteristics

A preliminary analysis of the met-mast data is performed to highlight key characteristics of the test site. Reference wind speed, wind direction, and turbulence intensity are computed using the met-mast instrumentation located at hub height. Turbulence intensity is calculated from the wind speed recordings sampled at 50 Hz.

Vertical wind shear is estimated by fitting a power-law profile to the two wind speed measurements available from the met mast, according to

$$\alpha_{\mathrm{mm}} = \frac{\log(U_{\mathrm{HH}}/U_{\mathrm{LB}})}{\log(z_{\mathrm{HH}}/z_{\mathrm{LB}})}, \tag{1}$$

where $U_{\mathrm{HH}}$ and $U_{\mathrm{LB}}$ denote the wind speeds measured at hub height (HH) and near the lower blade tip (LB), respectively. The resulting shear exponent is denoted by $\alpha$, with the subscript $\mathrm{mm}$ indicating that it is derived from met-mast measurements. The horizontal wind direction veer is computed as

$$\Delta\theta = \frac{\theta_{\mathrm{HH}} - \theta_{\mathrm{LB}}}{z_{\mathrm{HH}} - z_{\mathrm{LB}}} D, \tag{2}$$

where $\theta_{\mathrm{HH}}$ and $\theta_{\mathrm{LB}}$ are the wind directions measured at HH and LB, respectively. The quantity $\Delta\theta$ represents the variation in wind direction over the lower half of the rotor, linearly extrapolated to the full rotor diameter. A positive value of $\Delta\theta$ indicates that the wind direction rotates clockwise with increasing altitude above the terrain – as viewed from above.

It is well known that the vertical distribution of wind direction cannot, in general, be accurately represented by a linear profile, as it depends in a complex manner on atmospheric stability conditions. Consequently, the presence of veer in the lower part of the rotor does not necessarily imply veer over the upper part, nor that the veer profile is linear (Gao et al., 2021). Nevertheless, this simplified metric is used throughout the paper as an indicator of veering conditions at the test site, consistent with previous studies (Murphy et al., 2020; Englberger and Lundquist, 2020; Gomez and Lundquist, 2020).

To illustrate the relationship between shear and veer for winds originating from the southwest, a bivariate histogram is generated and shown in Fig. 2. The data are further grouped into wind-shear bins of width 0.1, and both the median wind veer and the corresponding interquartile ranges are displayed. A clear correlation between these two quantities emerges, particularly for shear values between 0.1 and 0.45. More stable atmospheric conditions generally lead to higher values of both shear and veer, as well as lower turbulence intensity (TI), which is omitted here for brevity. Overall, the wind field is characterized by frequent occurrences of high wind shear and by a long positive tail in the distribution of wind veers, consistent with the Northern Hemisphere Ekman spiral (Holton, 2004) under stable conditions. These results are considered sufficient to support the discussion presented in the paper; a more detailed description of the wind-gradient characteristics at this site can be found in Appendix A.

As shown in Sect. 4.4, the relationship between shear and veer can be leveraged to reduce the prediction error of wake models and to limit the number of inflow variables required when developing shear- and veer-aware wake-steering strategies.

https://doi.org/10.5194/wes-2026-93
Preprint. Discussion started: 29 June 2026


eawe european academy of wind energy
Open Access WIND ENERGY SCIENCE DISCUSSIONS

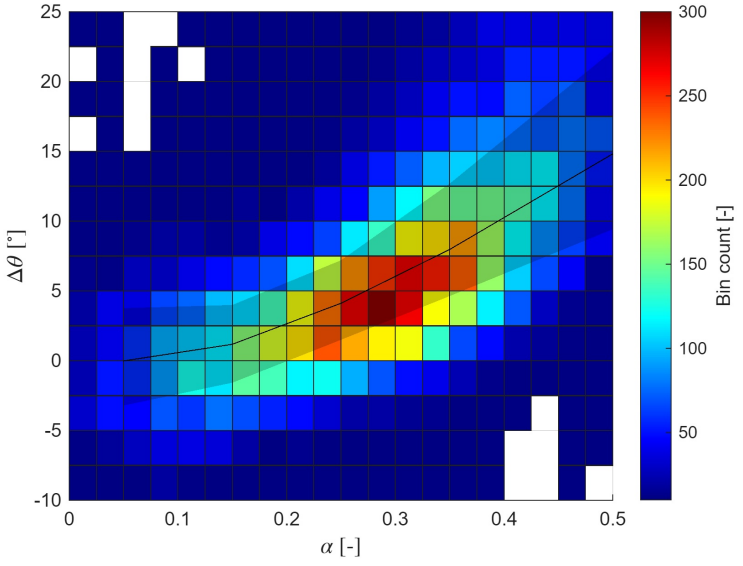


**Figure 2.** Relationship between met-mast-measured power-law shear exponent $\alpha$ and veer $\Delta\theta$ across the turbine rotor diameter, for south-westerly winds. The black solid line indicates the median wind veer, while the shaded area around it the interquartile range. White areas represent bins with null counts.

### 2.3 Analysis of SCADA data

A first analysis of the collected dataset aims to demonstrate the overall effect of vertical wind shear on the power production of the downstream turbine. This is done by examining the power output of WT2, normalized by the power generated by WT1. Excessive misalignments caused by poor wind-vane calibration on WT1 are removed from the dataset, as described in Sect. 2.1. For simplicity, the symbol $\alpha$ will hereafter denote the met-mast wind shear (instead of $\alpha_{\mathrm{mm}}$).

Figure 3 shows the power deficit of WT2 as a function of met-mast wind direction at hub height, grouped into bins of increasing wind-shear magnitude. Each subplot includes the corresponding fitted Gaussian curve, while the shaded areas represent the 95% confidence intervals – derived by bootstrapping the data 1,000 times – of both the fitted curve and the location of its minimum.

Using power ratios to estimate wake position has both advantages and limitations. A clear advantage is that this quantity can be readily computed from SCADA datasets and predicted by wind-farm engineering flow models. Moreover, turbine power inherently reflects inflow conditions across the entire rotor area, making it an integral measure. However, it is important to recall that, although power ratios have been used in previous studies (Vollmer et al., 2016; Schottler et al., 2017), they remain an indirect method for characterizing the inflow at a downstream turbine, and therefore cannot fully capture the complex wake structure.

https://doi.org/10.5194/wes-2026-93
Preprint. Discussion started: 29 June 2026


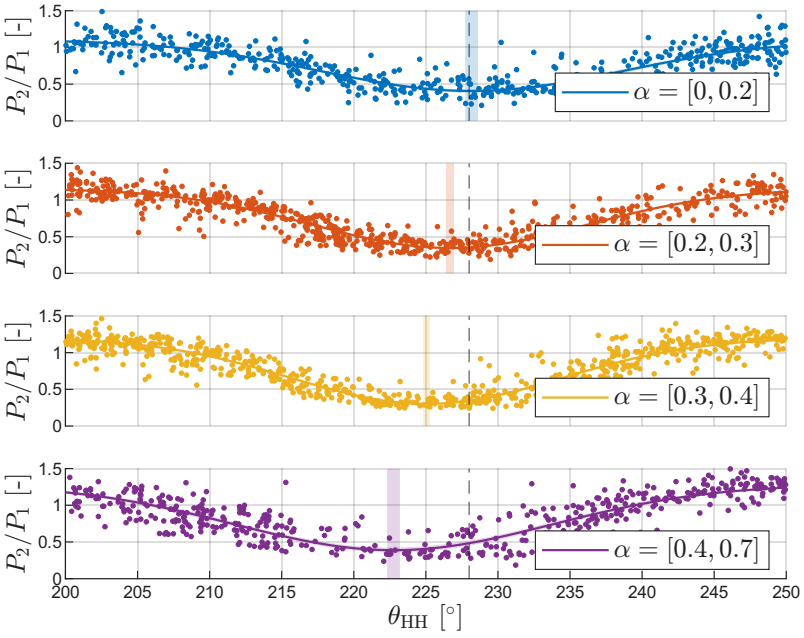


**Figure 3.** Power ratio $P_2/P_1$ plotted as a function of met-mast wind direction, binned for increasing vertical wind shears. Shaded areas represent the 95% confidence intervals of both the fitted curve and the location of its minimum. Vertical dashed lines indicate the direction for which the two turbines are geometrically aligned.

Figure 3 illustrates that the wake of WT1 undergoes a lateral displacement as the wind shear increases. As $\alpha$ increases, the position of the wake minimum clearly shifts toward lower wind directions, corresponding to a wake deflection to the right when viewed downstream. A crucial point, however, is that this displacement reflects the combined influence of wind shear and wind-direction veer, given the correlation shown in Fig. 2. To disentangle these effects, additional analyses are performed.

### 2.3.1 Influence of vertical wind shear

An analysis similar to the previous one is carried out here, selecting only data for which the wind veer lies within the range $-4° < \Delta\theta < +4°$. This restriction is applied to help disentangle the effects of veer and shear on wake displacements, while still ensuring a sufficient number of data points for statistical significance.

The behavior in Fig. 4 mirrors that of Fig. 3, albeit with slightly smaller wake deflections. This reduction is consistently reproduced across different wind-speed bins and data-averaging intervals, and is here attributed solely to the influence of a sheared inflow. Such shear-induced wake shifts have previously been highlighted in CFD studies by several authors (Fleming et al., 2014a; Vollmer et al., 2016; Gebraad et al., 2016b; Bromm et al., 2017). Proposed mechanisms include the advection of a counter-rotating, sheared wake and the interaction of this sheared wake with the ground. As shown later in Sect. 3.2, here we develop an alternative explanation based on a lateral force component proportional to wind shear. Within the present analysis, however, power-ratio data alone do not allow us to determine which mechanism is dominant.

https://doi.org/10.5194/wes-2026-93
Preprint. Discussion started: 29 June 2026


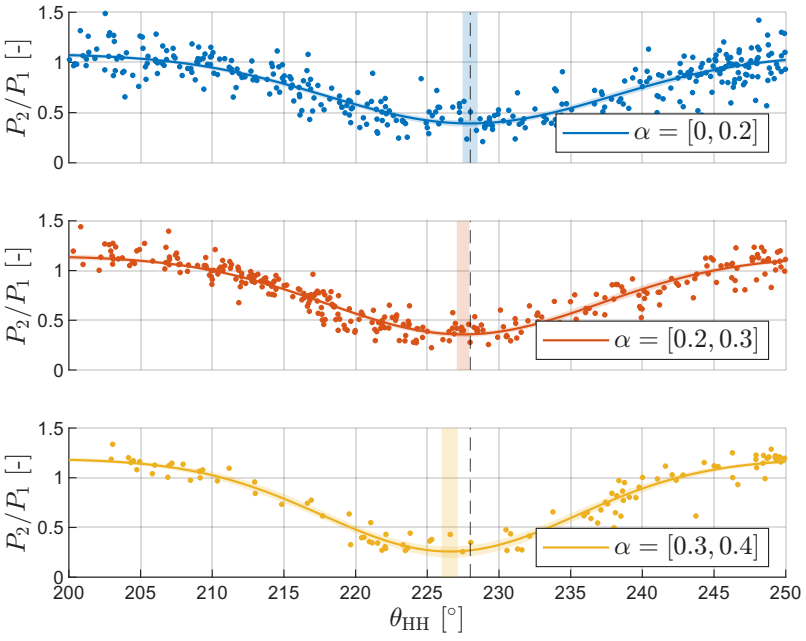


**Figure 4.** Power ratio $P_2/P_1$ plotted as a function of met-mast wind direction, for wind veers limited to $-4° < \Delta\theta < +4°$, binned for increasing vertical wind shear. Shaded areas represent the 95% confidence intervals of both the fitted curve and the location of its minimum. Vertical dashed lines indicate the direction for which the two turbines are geometrically aligned.

### 2.3.2 Influence of directional wind veer

A similar approach to that used in Sect. 2.3.1 is applied here to isolate the impact of wind veer. To this end, only data with vertical wind shears in the range $0.25 < \alpha < 0.4$ are considered. The results, shown in Fig. 5, indicate that wind veer induces a shift of the maximum power deficit toward lower wind directions, i.e. toward the right when looking downstream.

A positive wind-direction veer indeed has the effect of skewing the wake clockwise when viewed downstream (Vollmer et al., 2016), as schematically illustrated in Fig. 6. Because the downstream turbine is approximately 20 m (about 0.16 D) taller than the upstream turbine, its inflow is primarily influenced by the portion of the wake originating from the upper part of the rotor of WT1. Under positively veered inflow conditions, this leads to the downstream turbine experiencing a wake displaced toward the right when looking downstream.

### 2.3.3 Combined effects of shear and veer

So far, the analysis has focused on investigating the influence of shear and veer individually, showing qualitatively that each parameter contributes to displacing the wake released by WT1 toward the right when viewed downstream (although it is important to recall that the apparent deflection caused by veer is due to the different hub heights of the turbines, a peculiar characteristic of this test cluster). To provide a more comprehensive overview of these combined effects, the experimental data

https://doi.org/10.5194/wes-2026-93
Preprint. Discussion started: 29 June 2026


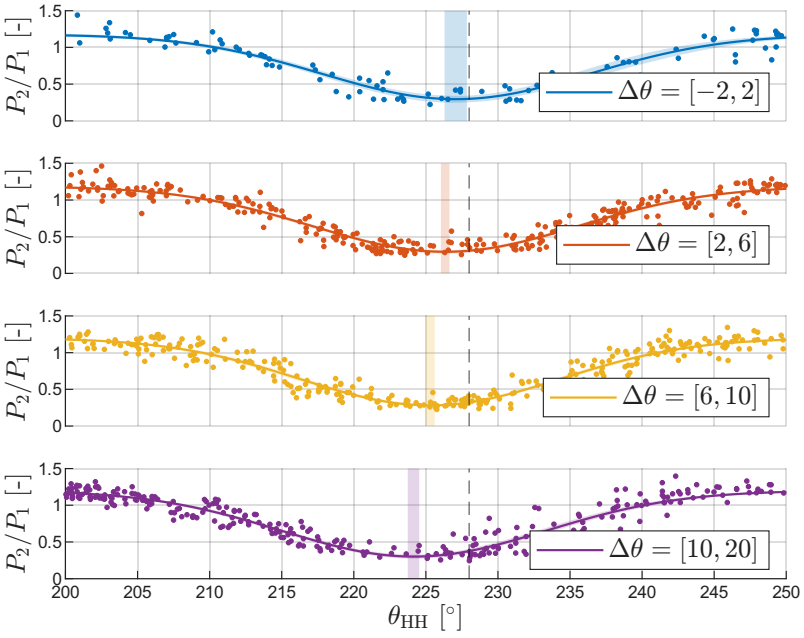


**Figure 5.** Power ratio $P_2/P_1$ plotted as a function of met-mast wind direction, for vertical wind shears limited to $0.25 < \alpha < 0.4$, binned for increasing veer. Shaded areas represent the 95% confidence intervals of both the fitted curve and the location of its minimum. Vertical dashed lines indicate the direction for which the two turbines are geometrically aligned.

are now binned simultaneously according to both shear and veer. Overlapping windows are applied between adjacent bins to ensure a sufficient number of samples in each group. The wind-shear bins, defined in terms of the shear-law exponent, have a width of 0.1, with bin centers spaced 0.025 apart. Wind veer is binned using 10°-wide windows, with centers spaced 2.5° apart.

For each two-dimensional bin, the position of the wake centerline is estimated by fitting the power-deficit data with a Gaussian curve. The turbine separation and the wind direction corresponding to turbine alignment are computed from their GPS coordinates. The wind-direction offset with respect to the line passing through the turbines is then converted into a lateral displacement using

$$\Delta y_{\mathrm{wc,fit}} = -r_{\text{1-2}} \sin(\theta_{\mathrm{wc,fit}} - \theta_{\text{1-2}})/D, \tag{3}$$

where $r_{\text{1-2}}$ is the distance between the turbines (336 m), $\theta_{\mathrm{wc,fit}}$ is the wind direction corresponding to the minimum of the fitted Gaussian (i.e. the wake centerline), and $\theta_{\text{1-2}}$ is the wind direction for which the turbines are aligned (approximately 228°). Because the deviations between $\theta_{\mathrm{wc,fit}}$ and $\theta_{\text{1-2}}$ are small, variations in the term $\cos(\theta_{\mathrm{wc,fit}} - \theta_{\text{1-2}})$ are neglected. Under the present sign convention, a positive value of $\Delta y_{\mathrm{wc,fit}}$ corresponds to a wake displacement toward the right when viewed downstream.

https://doi.org/10.5194/wes-2026-93
Preprint. Discussion started: 29 June 2026


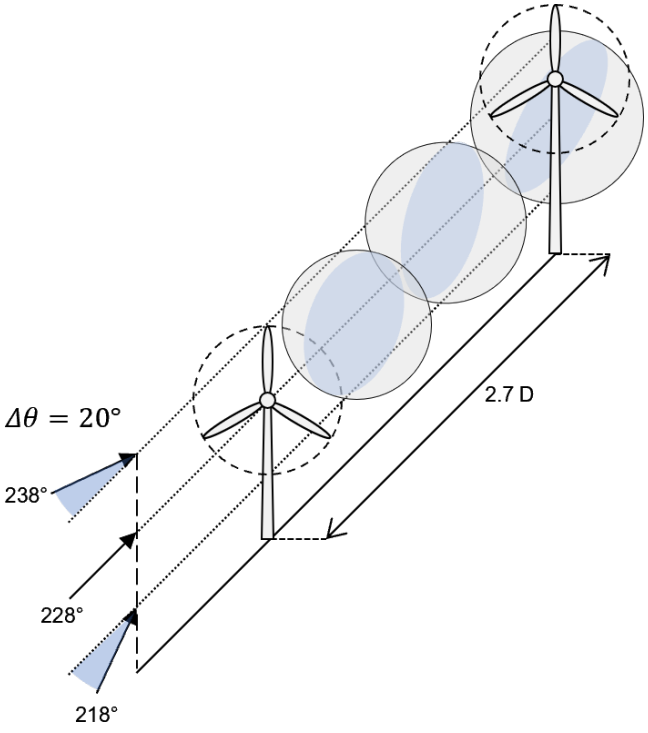


**Figure 6.** Sketch illustrating the effect of a positive wind veer on the wake interaction between turbines with different hub heights. A positive veer causes the wake to be stretched into an ellipsoid that rotates clockwise when viewed downstream, resulting in the downstream turbine – being taller – intersecting the upper, laterally shifted portion of the upstream wake. The resulting impact on its power production is equivalent to a wake displacement toward the right when looking downstream.

The results are shown in Fig. 7. Only data points for which the confidence interval is smaller than 0.05 D are displayed. The plot confirms the trends discussed in the previous sections. When shear and veer occur simultaneously – which is expected in practice, given their correlation shown in Sect. 2.2 – the combined effect can lead, in extreme cases, to very significant wake displacements, reaching values of roughly 0.3 D. The magnitude of these wake shifts is large, especially considering that the turbine spacing is only 2.7 D.

Figure 7 shows that, even in the absence of veer, variations in shear alone can displace the wake centerline by up to approximately 0.06 D. Using the FLORIS framework described in Sect. 3.4, it was found that an equivalent displacement is produced by a relatively modest +13.0° yaw misalignment under a representative turbulence intensity of 10%. Since Fig. 7 shows that much larger displacements can occur for higher combinations of shear and veer, it is reasonable to expect that neglecting wake shifts induced by these atmospheric parameters would be detrimental to the accuracy of any assessment of power output (and possibly even of turbine loads).

The findings of this section clearly highlight the significant impact of wind gradients on the power production of the downstream turbine. Similar trends were observed when using alternative normalization approaches – namely, replacing the power

https://doi.org/10.5194/wes-2026-93
Preprint. Discussion started: 29 June 2026




eawe european academy of wind energy
Open Access WIND ENERGY SCIENCE DISCUSSIONS

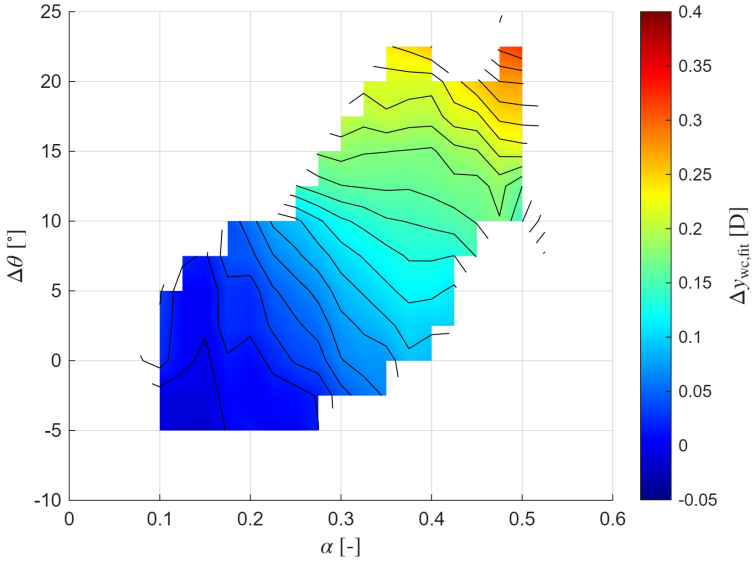


**Figure 7.** Wake displacement $\Delta y_{\mathrm{wc,fit}}$ as function of met-mast shear $\alpha$ and veer $\Delta\theta$.

ratio with the ratio of wind speeds measured by the onboard anemometers, or by normalizing the downstream power using the met-mast wind speed. Clearly, lateral wake displacement represents only one of the mechanisms through which shear and veer influence a downstream turbine. Other effects – such as changes in wake recovery, wake turbulence, and the differences in structural loading associated with a skewed versus a straight wake – are also important. However, a comprehensive assessment of these additional impacts lies beyond the scope of the present work and is left for future research.

## 3 Models

### 3.1 High-fidelity CFD model

High fidelity CFD analyses are conducted to investigate some open questions arising from the results presented so far, namely:

- Because shear and veer simultaneously influence wake position, it is generally not possible to isolate the effect of each parameter alone from free-field experiments.
- It remains unclear whether the findings reported in Sect. 2.3.1 are partly or entirely influenced by other effects such as complex terrain, vegetation, or unaccounted turbine operating conditions.
- The power ratio $P_2/P_1$ provides only an indirect representation of the wake and does not capture its detailed structure. CFD simulations, by contrast, offer direct visualization of the flow field and therefore enable a more comprehensive assessment of wake development.

https://doi.org/10.5194/wes-2026-93
Preprint. Discussion started: 29 June 2026


eawe european academy of wind energy
Open Access WIND ENERGY SCIENCE DISCUSSIONS

In addition, high-fidelity CFD simulations can be used to verify and validate the predictions of simplified engineering models.

Simulations are performed using a TUM-modified version of NREL's large-eddy simulation with actuator line model (LES-ALM) Simulator fOr Wind Farm Applications (SOWFA) (Fleming et al., 2014a; Wang et al., 2019). The incompressible solver is based on a finite-volume formulation and uses a standard Smagorinsky model to treat subgrid scales, with a constant of 0.13 (Sagaut, 2006).

The LES Cartesian mesh comprises approximately 14.5 million cells and includes 4 refinement levels. The smallest cells measure 1 m and are located in correspondence with the rotor.

Unsteady tests are run with TurbSim-generated turbulent winds (TurbSim, 2023), which are injected into the domain using the OpenFOAM (Greenshields, 2018) *"timeVaryingMappedFixedValue"* boundary conditions. Inflows are characterized by a turbulence intensity TI$= 3\%$, a hub height freestream wind speed $U_\infty = 8.5$ ms$^{-1}$, and values of the power-law shear coefficient equal to $[0, 0.2, 0.4, 0.6]$. Each LES-ALM simulation is run for 950 seconds. The first 300 seconds are considered as the initial transient, and hence they are discarded.

Simulations are conducted on a modified version of the IEA 3.35 MW reference wind turbine (RWT) (Bortolotti et al., 2019), whose main parameters are summarized in Table 1.

**Table 1.** Main specifications of the IEA 3.35 MW RWT.

| Data | Value |
|---|---|
| Wind class | IEC 3A |
| Control | Variable speed, collective pitch |
| Rated electrical power | 3.35 MW |
| Hub height | 110.0 m |
| Rotor diameter | 130.0 m |
| Rotor cone angle | 0.0° |
| Nacelle uptilt angle | 0.0° |

### 3.2 Shear-induced lateral force model

Classical models of wake deflection explain the lateral shift of a wake as caused by a lateral force component exerted on the flow by the rotor (Jiménez et al., 2010). When a rotor is misaligned with respect to the wind, this force mainly arises from the lateral projection of the thrust force $T$. Building on this concept, the additional contribution of the side (rotor-in-plane) force $S$ can be included, leading to a revised expression of Eq. (20) of Jiménez et al. (2010), which quantifies the initial wake skew angle relative to the incoming inflow:

$$\chi_0 = \frac{1}{2}\left(C_T \sin\gamma - C_S \cos\gamma\right), \tag{4}$$

https://doi.org/10.5194/wes-2026-93
Preprint. Discussion started: 29 June 2026


eawe european academy of wind energy
Open Access WIND ENERGY SCIENCE DISCUSSIONS

where $\gamma$ is the misalignment angle, $C_T = T/(qA)$ and $C_S = S/(qA)$ are respectively the thrust and side-force coefficients, where $q = 0.5\rho U_\infty^2$ is the dynamic pressure, $\rho$ the air density, and $A$ the rotor swept area. Equation (4) shows that, even for zero misalignment, the skew angle can differ from zero – and the wake is laterally displaced – if a side force is present, i.e. $\chi_0 \neq 0$ when $\gamma = 0°$ and $C_S \neq 0$. It should be noted that the expression in Eq. (20) of Jiménez et al. (2010) differs from that in Eq. (4) by a factor of $\cos^2\gamma$, due to a different definition of the thrust and side-force coefficients.

Vertical wind shear can indeed induce a non-zero lateral force on the rotor even in the absence of misalignment. This effect arises from the broken symmetry introduced by rotor rotation. In fact, when a blade travels from left to right (looking downstream) in the upper half of the rotor, it experiences a different velocity triangle than when it moves from right to left in the lower half, due to the variation of the rotor-normal inflow velocity with height. As a result, the rotor-in-plane lateral force generated in the upper half of the rotor does not exactly balance that produced in the lower half, leading to a net residual lateral force acting in the plane of the rotor. A similar effect on the velocity triangles is induced by wind veer; in this case, however, it arises from variations in inflow direction rather than in wind speed.

In the spirit of developing a simple and fast correction for engineering wake models, we seek an analytical expression for the shear-induced lateral force. To this end, we employ the model developed by Tamaro et al. (2024), which derives analytical expressions for the thrust and power of a misaligned wind turbine. The model is based on classical blade element momentum (BEM) theory and describes the streamtube generated by a misaligned rotor, obtaining the lateral sidewash by considering the rotor as a lifting wing operating at an angle of attack given by the misalignment angle. The resulting thrust and aerodynamic power are computed by integrating the normal and tangential sectional forces along the blade span and over a full rotor revolution. To obtain analytical force expressions, spanwise-equivalent values of the lift slope $C_{L,\alpha}$ and drag coefficient $C_D$ are introduced, which can be approximated by evaluating the actual spanwise-varying quantities at two-thirds of the blade span (Tamaro et al., 2024).

The details of the model are not provided here as they are not relevant for the present work. However, by projecting the tangential forces at blade sections in the horizontal direction, integration along the blade span and over a rotor revolution readily gives the lateral force $S$, positive toward the right when looking downstream. Using the results in Tamaro et al. (2024), the axial induction factor $a_0$ and the thrust coefficient $C_T$ are computed by solving the following set of coupled equations

$$1 - a_0 = \frac{1 + \sqrt{1 - C_T - \frac{1}{16} C_T^2 \sin^2\gamma}}{2\left(1 + \frac{1}{16} C_T \sin^2\gamma\right)}, \tag{5a}$$

$$C_T = \frac{\sigma}{2}\left( (C_D + C_{L,\alpha})\lambda\cos\gamma(1 - a_0) - C_{L,\alpha}\beta\left(\sin^2\gamma + \frac{2}{3}\lambda^2\right) \right.$$
$$\left. - k\left( (C_D + C_{L,\alpha})\sin\gamma\cos\gamma(1 - a_0) - \frac{2}{3} C_{L,\alpha}\beta\lambda\sin\gamma \right) - \frac{k^2}{4} C_{L,\alpha}\beta\sin^2\gamma \right), \tag{5b}$$

where $\sigma$ is the rotor solidity, $k$ is the vertical shear linear coefficient, $\lambda$ is the tip speed ratio, and $\beta$ is the pitch angle. In contrast to Tamaro et al. (2024), the present results neglect rotor tilt for simplicity. As explained in Sect. 3.3 of Tamaro et al. (2024), these equations can be solved while accounting for the turbine control strategy when yawing away from the wind.

https://doi.org/10.5194/wes-2026-93
Preprint. Discussion started: 29 June 2026


eawe european academy of wind energy
Open Access WIND ENERGY SCIENCE DISCUSSIONS

Once $a_0$ and $C_T$ have been computed from Eq. (5), the side force coefficient $C_S$ is obtained as

$$C_S = \frac{\sigma}{2}\Bigg( - C_D\lambda\sin\gamma - C_{L,\alpha}\beta\sin\gamma\cos\gamma(1-a_0) \\ - k\left(C_{L,\alpha}\cos^2\gamma(1-a_0)^2 - \frac{3}{4}C_D\sin^2\gamma - \frac{1}{3}C_{L,\alpha}\beta(1-a_0)\lambda\cos\gamma\right) - \frac{k^2}{4}C_{L,\alpha}\beta\sin\gamma\cos\gamma(1-a_0)\Bigg). \quad (6)$$

It is interesting to observe that – as expected – the lateral force coefficient $C_S$ depends on the shear coefficient $k$, and that $C_s$ remains non-zero even for a null misalignment angle $\gamma$, and in fact

$$C_{S_{\gamma=0^\circ}} = -k\frac{\sigma}{2}C_{L,\alpha}(1-a_0)\left(1-a_0-\frac{1}{3}\beta\lambda\right). \quad (7)$$

For small pitch angles $\beta$, $C_S$ becomes increasingly negative as the shear coefficient $k$ increases. Since $S$ is the force on the rotor, the force exerted on the flow is directed toward the right when looking downstream, which implies that the wake is deflected to the right in agreement with Eq. (4) and the findings discussed in Sect. 2.

### 3.3 Shear-induced lateral displacement

This section addresses whether the shear-induced lateral force derived above can explain the observed lateral wake displacement. We first assess the accuracy of the force predicted by the analytical model by comparing it with the force obtained from the CFD simulations. For the model predictions, the values $\sigma = 0.0418$, $C_{L,\alpha} = 4.75$ rad$^{-1}$, and $C_D = 0.004$ were used in Eqs. (5) and (6). The force from the CFD simulations was computed by numerically integrating the lateral aerodynamic force along the span of the three blades and subsequently averaging it over the final 10 rotor revolutions.

The results are shown in Fig. 8a, which reports the lateral force coefficient $C_S$ as a function of the shear exponent $\alpha$. A good agreement is observed between the model predictions and the CFD results, although discrepancies increase at higher shear values. This behavior is likely attributable to the use of a linear shear coefficient $k$ in the analytical model, as opposed to the logarithmic velocity profile prescribed in the CFD simulations. Overall, $C_S$ is zero in the absence of shear and increases in magnitude with increasing shear, giving rise to the lateral force discussed in the previous section.

To provide a more quantitative assessment of the wake displacements predicted by the model, the lateral displacement of the wake centerline, $\Delta y_{\mathrm{wc}}$, is computed by integrating the skew angle $\chi$ in the downstream direction according to Jiménez et al. (2010):

$$\chi(x) = \frac{1}{2}\frac{C_T\sin\gamma - C_S\cos\gamma}{1+\xi x/D}, \quad (8a)$$

$$\Delta y_{\mathrm{wc}}(x) = \int_0^x \tan\left(\chi(x')\right)\mathrm{d}x', \quad (8b)$$

where $x$ denotes the downstream distance from the turbine, $\xi = 0.075$ is the linear wake expansion coefficient, and $x'$ is a dummy integration variable. In the present case, since the misalignment angle $\gamma$ is zero, the lateral wake displacement is solely induced by the lateral force coefficient $C_S$.

https://doi.org/10.5194/wes-2026-93
Preprint. Discussion started: 29 June 2026


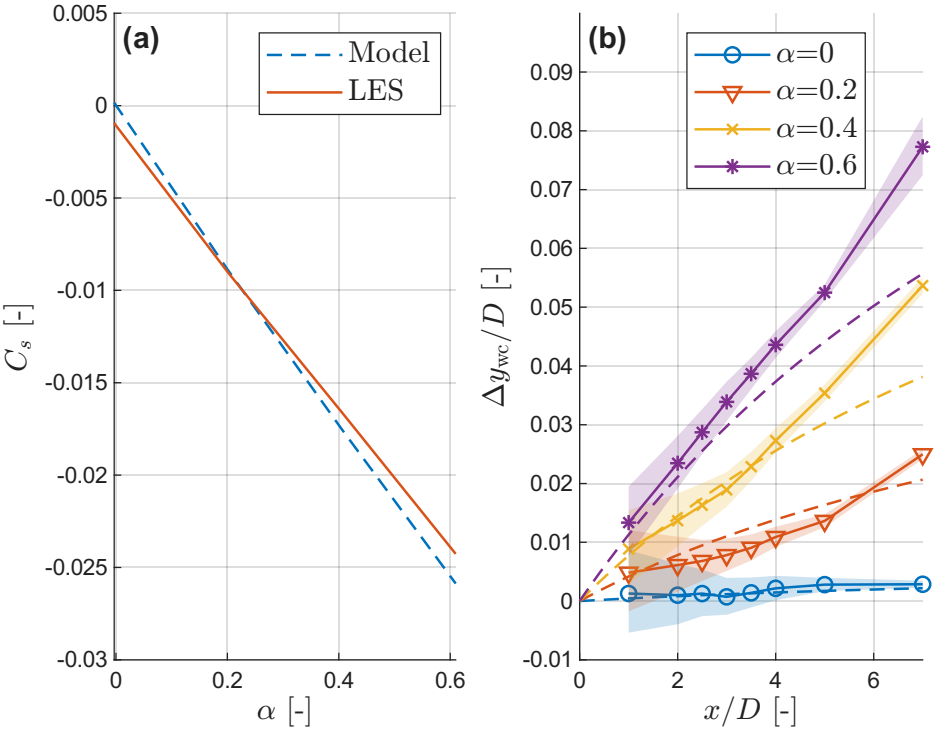


**Figure 8.** Comparison between the lateral force coefficient $C_S$ obtained from LES (red solid line) and from the analytical model (blue dashed line) for increasing shear exponents $\alpha$ **(a)**. Comparison of wake centerline displacements $\Delta y_{\mathrm{wc}}$ as a function of downstream distance for various shear exponents $\alpha$ **(b)**. Centerline displacements obtained integrating the skew angle via Eq. (8) using LES-based $C_S$ are shown as dashed lines, while displacements calculated by minimizing $U_{\mathrm{REWS},2}$ are shown as solid lines. Shaded regions indicate 95% confidence intervals.

The wake displacement in the CFD simulations is determined using the following procedure. First, longitudinal wind velocity fields are extracted at several downstream locations between 1 and 7 D. For each downstream plane, the normalized rotor-equivalent wind speed, $U_{\mathrm{REWS},2}$, of a virtual downstream turbine located at hub height is computed. This calculation is repeated for different lateral positions of the virtual turbine, and the wake centerline location is identified as the lateral position corresponding to the minimum value of $U_{\mathrm{REWS},2}$. The minimum is determined by fitting a Gaussian function to the $U_{\mathrm{REWS},2}$ distribution.

Figure 8b shows a comparison between the lateral displacements predicted by integrating Eq. (8), using the $C_S$ obtained from LES simulations, and those calculated by minimising $U_{\mathrm{REWS},2}$. Lateral displacements are shown as a function of downstream distance, for increasing shear exponents.

Several conclusions can be drawn from the figure:

- The LES simulations confirm the general trend observed in the field experiments, with the wake centerline shifting to the right in the presence of vertical shear.

https://doi.org/10.5194/wes-2026-93
Preprint. Discussion started: 29 June 2026


eawe european academy of wind energy
Open Access WIND ENERGY SCIENCE DISCUSSIONS

- The wake displacement $\Delta y_{\mathrm{wc}}$ estimated from the lateral force coefficient $C_S$ using Eq. (8) agrees reasonably well with that obtained from $U_{\mathrm{REWS},2}$, particularly for low shear values and in the near to mid wake. This indicates that $C_S$ can be used as a practical estimator of shear-induced wake displacement.

- In the far wake and for $\alpha > 0.4$, the CFD simulations predict larger lateral displacements than those obtained from the model. This discrepancy is partly attributable to the emergence of complex wake structures at high shear levels, which are not captured by the simplified model. Additional limitations arise from the assumption of a linear wake expansion and from the use of a single, rotor-averaged lateral force coefficient, whereas in reality $C_S$ varies across the rotor disk.

- Visual inspection of the flow field (not shown here for brevity) reveals that wake rotation convects the vertical shear downstream, rotating it counter-clockwise and transporting low-momentum flow from the lower part of the rotor toward the right. This effect is particularly evident in the near wake, gradually weakening as the wake becomes fully developed and the influence of shear diminishes, eventually disappearing. Although its influence on the estimated wake displacement appears limited in the present case, its modeling and quantitative assessment represent promising directions for future research.

Lastly, we compare the wake displacements measured in the field experiments – primarily attributed to wind shear – with those predicted by the LES simulations. In the numerical analysis, the virtual downstream turbine is sampled at a height of 0.16 D above the upstream hub height, thereby preserving the geometric proportions of the free-field experiments. The results are presented in Fig. 9.

While the general trend of increasing wake displacement with shear exponent is consistent between experiments and LES, the field measurements exhibit larger displacements than those predicted by the simulations, particularly at higher shear exponents.

Several factors may contribute to these discrepancies:

- The LES simulations are performed on a reference IEA 3.35 MW wind turbine, which differs from the turbine used in the field experiments.

- In the field experiments, it is not possible to fully disentangle the respective contributions of shear and veer. As a result, the experimentally observed wake displacements are likely larger than those predicted by the LES simulations, which account for shear effects only.

- Low shear conditions in the field experiments are often associated with higher turbulence intensities, thereby increasing the uncertainty in the wake displacement estimates.

- Residual yaw misalignments of both the upstream and downstream turbines may still influence the measured wake displacements.

- Terrain-induced effects, such as hills and vegetation, are not represented in the LES simulations and may further affect wake behavior.

https://doi.org/10.5194/wes-2026-93
Preprint. Discussion started: 29 June 2026


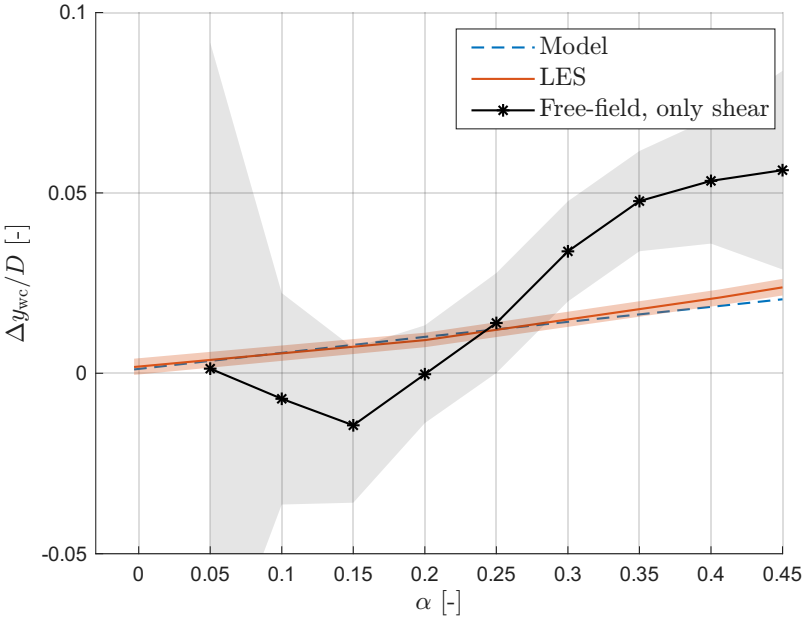


**Figure 9.** Non-dimensional lateral wake displacement, $\Delta y_{\mathrm{wc}}/D$, as a function of the shear exponent $\alpha$. Predictions based on LES-derived $C_S$, obtained by integrating the skew angle using Eq. (8), are shown by the blue dashed line; LES results are shown by the red solid line; field measurements for $-4^\circ < \Delta\theta < +4^\circ$ are indicated by asterisks and the interpolating solid black line.

Despite these discrepancies, the LES simulations corroborate the general trend observed in the field experiments, namely a rightward shift of the wake centerline in the presence of wind shear.

### 3.4 Wake models

A numerical replica of the test site was implemented using the FLORIS framework (FLORIS, 2025). The turbine power curve was provided by the manufacturer, while the turbine locations – expressed in UTM coordinates – were obtained from GPS measurements. A brief overview of the wake models used in this study is presented below.

Since all considered models are based on a Gaussian formulation, the discussion focuses only on the terms governing the representation of wind veer and shear. Readers are referred to the original publications for full implementation details. Although more advanced wake models exist in the literature, the present work concentrates on non-misaligned inflow conditions and a simple two-turbine configuration. Under these conditions, the standard Gaussian model is adopted due to its simplicity and computational efficiency.

#### 3.4.1 Baseline wake model

The Gauss-Legacy model included within the FLORIS framework is used here as the baseline wake model (Annoni et al., 2018). This model originates from a series of studies, including Bastankhah and Porté-Agel (2014, 2016), Abkar and Porté-

https://doi.org/10.5194/wes-2026-93
Preprint. Discussion started: 29 June 2026


eawe european academy of wind energy
Open Access WIND ENERGY SCIENCE DISCUSSIONS

Agel (2015), and Niayifar and Porté-Agel (2016), among others. In this formulation, the effect of wind veer is incorporated by applying a rotation factor to the Gaussian wake distribution (see Eq. 10 in the original publication).

The longitudinal wind speed within the wake is expressed as

$$\frac{u(x,y,z)}{U_\infty} = 1 - C(x)e^{-(\ell_y(y-\Delta y_{\mathrm{wc}})^2 - 2\ell_{yz}(y-\Delta y_{\mathrm{wc}})(z-z_{\mathrm{HH}}) + \ell_z(z-z_{\mathrm{HH}})^2)}, \tag{9a}$$

$$\ell_y = \frac{\cos^2\psi}{2\sigma_y^2} + \frac{\sin^2\psi}{2\sigma_z^2}, \tag{9b}$$

$$\ell_{yz} = -\frac{\sin 2\psi}{4\sigma_y^2} + \frac{\sin 2\psi}{4\sigma_z^2}, \tag{9c}$$

$$\ell_z = \frac{\sin^2\psi}{2\sigma_y^2} + \frac{\cos^2\psi}{2\sigma_z^2}, \tag{9d}$$

where $C(x)$ denotes the maximum velocity deficit, which depends on the downstream distance $x$ from the rotor, the thrust coefficient, and the turbulence intensity. The term inside the exponential of Eq. (9a) defines the shape of the Gaussian distribution, centered at the hub height $z_{\mathrm{HH}}$ and laterally displaced by $\Delta y_{\mathrm{wc}}$. The parameters $\ell_y$, $\ell_{yz}$, and $\ell_z$ describe the rotation of the elliptical contours, which in the present model is prescribed by the veer-dependent angle $\psi$. Notice that the model assumes a constant rotation of the wake across its entire length.

The effect of vertical shear is limited to a modification of the background inflow profile and therefore does not directly influence either the wake deficit or the wake deflection.

The lateral wake displacement in zero yaw conditions is modeled by the two parameters $a_d$ and $b_d$ through the expression:

$$\Delta y_{\mathrm{wc}}(x) = a_d + b_d x. \tag{10}$$

The Gauss-legacy model further depend on the parameters $N_{\mathrm{gauss},\alpha}$, $N_{\mathrm{gauss},\beta}$, $K_a$, $K_b$, which govern the evolution of the wake velocity deficit and the extension of the near wake. These parameters are not modified nor reformulated in the following, and therefore the interested reader is referred to Annoni et al. (2018) and the underlying wake formulations for a more precise description of their role in the governing model equations.

### 3.4.2 Abkar veer wake model

In Abkar et al. (2018), a model is proposed that relates the skewness of the wake both to the intensity of the incoming wind veer and to the downstream distance from the rotor. The lateral displacement of the wake is defined as

$$\Delta y_{\mathrm{wc}}(x,z) = a_d + (b_d + \tan(\theta(z) - \theta_{\mathrm{HH}}))\, x, \tag{11}$$

where $\theta(z)$ is the incoming wind direction at height $z$. This formulation enables the representation of arbitrary veer profiles across the rotor disk, following an approach analogous to that of Gebraad et al. (2016a).

This formulation has been incorporated into the present FLORIS implementation as a modification of the baseline model described in Sect. 3.4.1 and is hereafter referred to as the Abkar veer (AV) model.

https://doi.org/10.5194/wes-2026-93
Preprint. Discussion started: 29 June 2026


eawe european academy of wind energy
Open Access WIND ENERGY SCIENCE DISCUSSIONS

The difference between the baseline and the AV models can be summarised as follows: the baseline model assumes that the veer-induced wake rotation $\psi$ is uniform throughout the entire wake, whereas in the AV model the wake skew varies linearly with downstream distance from the rotor. The angle $\psi$ that must be applied in the baseline model to reproduce the same wake rotation predicted by the AV model can be obtained through straightforward algebraic manipulation:

$$\psi \approx \arctan(x\Delta\theta/D), \tag{12}$$

where $\Delta\theta$ is the difference in wind direction across the rotor.

It is worth noting that the AV model does not rotate the two-dimensional Gaussian function. Instead, it stretches the wake laterally in the $y$ direction. Consequently, whereas wind veer does not alter the lengths of the principal axes of the elliptical wake contours in the baseline Gaussian model, it does modify them in the AV model. As a consequence, the veer-induced skew is much more pronounced in the AV model than in the baseline one. More details on the differences between the models are provided in Appendix B.

#### 3.4.3 Augmented Abkar veer model

This new model variant is designed to incorporate the influence of wind shear on the lateral wake displacement observed in Sect. 2.3 and Sect. 3.2. We achieve this by "augmenting" the AV model described in Sect. 3.4.2, such that the deflection parameter $a_d$ of Eq. (10) – which dictates the initial lateral shift of the wake – follows a shear-dependent linear relationship:

$$a_d(\alpha) = (M_1\alpha + M_2)D. \tag{13}$$

The constants $M_1$ and $M_2$ are determined experimentally, as described in Sect. 4.4. Since this variant is a modification of the AV model, it is indicated in the following with the label $\mathrm{AV}_{\mathrm{augm}}$.

#### 3.4.4 Augmented Abkar veer model with veer correlated to met-mast shear

The aim of this second model variant is to assess whether the observed correlation between wind shear and wind veer can be used to reduce the number of inflow parameters required by the wake model. Reducing the number of necessary inflow parameters clearly simplifies model usage.

To explore this possibility, a relationship between shear and veer is derived from Fig. 2, where a second-order polynomial fit yields the following expression for wind veer as a function of shear:

$$\Delta\theta(\alpha_{\mathrm{mm}}) = 33.73\,\alpha_{\mathrm{mm}}^2 + 19.75\,\alpha_{\mathrm{mm}} - 2.36. \tag{14}$$

The subscript $(\cdot)_{\mathrm{mm}}$ indicates that shear and veer are obtained from met mast measurements.

Clearly, this relationship is site-specific, and developing a more universally applicable model lies beyond the scope of the present work. The expression can be incorporated into any of the previously presented wake models without requiring modifications to their underlying formulations. The augmented AV model employing the veer predicted by Eq. (14) is denoted $\mathrm{AV}_{\mathrm{augm},\Delta\theta(\alpha_{\mathrm{mm}})}$ in the remainder of the paper.

https://doi.org/10.5194/wes-2026-93
Preprint. Discussion started: 29 June 2026


eawe european academy of wind energy
Open Access WIND ENERGY SCIENCE DISCUSSIONS

#### 3.4.5 Augmented Abkar veer model with veer correlated to observed shear

If a veer-shear-aware model is to be used in a control environment, these inflow parameters must be estimated in real time during turbine operation. The solution just described in Sect. 3.4.4 is not directly suitable for this purpose, as met masts are not routinely installed at wind farms and – even when they are – their measurements are not co-located with the turbines.

To provide this capability, we rely on the "rotor as a sensor", a technique that infers aerodynamic inflow characteristics from operational SCADA data and blade-load measurements. Over the years, a variety of wind-sensing approaches have been developed, ranging from estimating the rotor-effective wind speed (REWS) via the torque-balance equation (Ma et al., 1995), to more advanced estimators capable of predicting wind direction and shear across the rotor disk (Kim et al., 2023). In Schreiber et al. (2020a), out-of-plane bending moments are used to estimate the local wind speed experienced by each blade, yielding both vertical and horizontal shear estimates. Another approach – first proposed by Bottasso and Riboldi (2014) and further developed in Bertelè and Bottasso (2020); Bertelè et al. (2021) – uses blade-load harmonics to estimate vertical and horizontal shear as well as wind tilt and yaw misalignment.

In this work, we employ the wind estimator presented and validated in Kim et al. (2023), which uses a feed-forward neural network (NN) to map blade-load harmonics into wind-state estimates. Notably, if a turbine is already equipped with blade-load sensors, this estimator can be deployed without any additional hardware, and therefore comes at no additional cost.

The vertical shear exponent estimated from met-mast data ($\alpha_{\mathrm{mm}}$) is compared with the value obtained from the wind observer ($\alpha_{\mathrm{obs}}$) in Figs. 10a and 10b. As shown in Fig. 10a, the two estimates exhibit reasonably good agreement. A time history is shown in Fig. 10b, demonstrating that the observer is able to capture the general trend, including the diurnal cycle, of the wind shear.

Fitting a second-order polynomial to the observed shear, yields the following site-specific expression for wind veer as a function of shear:

$$\Delta\theta(\alpha_{\mathrm{obs}}) = 28.88\,\alpha_{\mathrm{obs}}^2 + 14.64\,\alpha_{\mathrm{obs}} - 0.52. \tag{15}$$

The subscript $(\cdot)_{\mathrm{obs}}$ indicates that shear and veer are obtained from the "rotor as a sensor" wind observer. The augmented AV model employing the veer predicted by Eq. (15) is denoted $\mathrm{AV}_{\mathrm{augm},\Delta\theta(\alpha_{\mathrm{obs}})}$ in the remainder of the paper.

#### 3.4.6 Summary of models

These various models and variants are shown in Table 2 and will be benchmarked against the experimental dataset in Sect. 4.3.

## 4 Results

### 4.1 Tuning of engineering wake model

A tuning of the wake-model parameters is now carried out. The procedure used to calibrate the model coefficients follows the approach first introduced in Bottasso et al. (2014); Schreiber et al. (2020b) and later extended in Braunbehrens et al. (2022), in which the tuning variables are transformed into a set of orthogonal parameters via singular value decomposition

https://doi.org/10.5194/wes-2026-93
Preprint. Discussion started: 29 June 2026


eawe european academy of wind energy
Open Access WIND ENERGY SCIENCE DISCUSSIONS

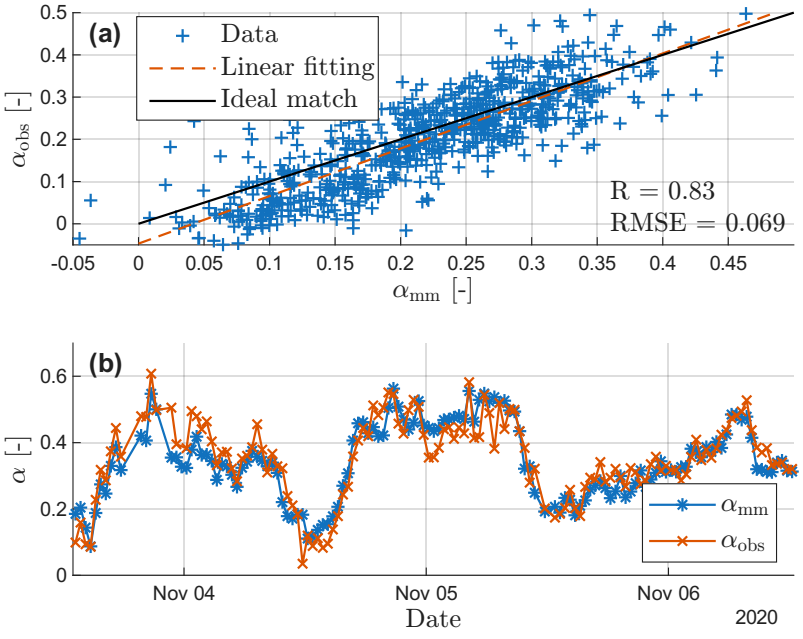


**Figure 10.** Comparison of vertical wind shear estimated from met-mast data ($\alpha_{\mathrm{mm}}$) and by the "rotor as a sensor" wind observer ($\alpha_{\mathrm{obs}}$) (Kim et al., 2023): correlation **(a)** and time history **(b)**.

**Table 2.** Overview of the main features of the wake models and their variants considered in this study.

| Wake model/variant | Veer-related wake skewing | $a_d$ | Veer input | N. of model inputs |
|---|---|---|---|---|
| baseline | Uniform | Constant | $\Delta\theta_{\mathrm{mm}}$ | 5 |
| AV | Progressive | Constant | $\Delta\theta_{\mathrm{mm}}$ | 5 |
| $\mathrm{AV}_{\mathrm{augm}}$ | Progressive | $a_d(\alpha_{\mathrm{mm}})$ | $\Delta\theta_{\mathrm{mm}}$ | 5 |
| $\mathrm{AV}_{\mathrm{augm},\Delta\theta(\alpha_{\mathrm{mm}})}$ | Progressive | $a_d(\alpha_{\mathrm{mm}})$ | $\Delta\theta(\alpha_{\mathrm{mm}})$ | 4 |
| $\mathrm{AV}_{\mathrm{augm},\Delta\theta(\alpha_{\mathrm{obs}})}$ | Progressive | $a_d(\alpha_{\mathrm{obs}})$ | $\Delta\theta(\alpha_{\mathrm{obs}})$ | 4 |

https://doi.org/10.5194/wes-2026-93
Preprint. Discussion started: 29 June 2026


eawe european academy of wind energy
Open Access WIND ENERGY SCIENCE DISCUSSIONS

(SVD). The optimization problem is solved in this orthogonal space, and the solution is subsequently mapped back onto the original parameter space. This technique makes it possible to identify the parameters that primarily influence the quality of the predictions, while discarding those that are unobservable from the dataset and would otherwise render the problem ill-posed. For a detailed discussion of the method, the interested reader is referred to Schreiber et al. (2020b) and Bottasso et al. (2014). In the present work, this tuning method is employed to determine the wake parameters that yield the best agreement between model predictions and experimental data, in terms of the WT2 power output.

Since all models discussed above are based on the same Gaussian formulation, the parameters requiring calibration are identical, namely $N_{\mathrm{gauss},\alpha}$, $N_{\mathrm{gauss},\beta}$, $K_a$, $K_b$, $a_d$, and $b_d$. Their initial values are set to the default ones.

Given the 2-turbine configuration of the test field, the parameters $a_d$ and $b_d$ of Eq. (10) effectively convey the same information. This is because the parameter $b_d$, which governs the downstream evolution of the lateral wake displacement, requires at least two distinct measurement locations for proper identification. For this reason, $b_d$ is not observable in the present setup and is therefore omitted in the remainder of the paper.

In principle, it is not possible to tune the individual wake parameters independently, as their effects are correlated and the SVD transformation produces tuning variables that are linear combinations of the original parameters. However, it was found that the parameter $a_d$ exhibits only weak correlation with the other four tunable parameters $N_{\mathrm{gauss},\alpha}$, $N_{\mathrm{gauss},\beta}$, $K_a$, and $K_b$, which govern the evolution of the wake velocity deficit and the extent of the near-wake region. Based on this observation, these four parameters are tuned once for the baseline model and subsequently kept fixed for all other models, thereby simplifying both the analysis and the comparison among models.

This procedure produced values of $N_{\mathrm{gauss},\alpha}$, $N_{\mathrm{gauss},\beta}$, $K_a$, and $K_b$ that remain very close to their default settings. The tuning of the baseline model further resulted in $a_d = -0.10$, representing the average wake displacement across all shear and veer conditions, as this model cannot account for displacement variations driven by these inflow characteristics.

### 4.2 Sensitivity to wind speed and wind direction estimates

The sensitivity of FLORIS outputs to different wind-speed and wind-direction estimates used as reference ambient conditions is assessed in this section using only the baseline wake model. Results remain consistent when the additional models presented in Sect. 3.4 are also employed, but are not shown here for brevity.

Results are presented by comparing the measured and simulated power of both wind turbines using the median absolute deviation (MAD), which provides a robust measure of prediction error. For improved interpretability, the MAD is normalized with respect to the median power output of each turbine.

The first analysis investigates the use of different measurements for the ambient wind speed. It is essential that the reference wind speed accurately represents the undisturbed inflow to the upstream turbine. Since the generated power is sensitive to the incoming wind speed, any mismatch between the reference value and the true inflow inevitably affects the predictive accuracy of the model. FLORIS predictions obtained using three different reference wind speeds are compared: the met-mast wind speed at hub height $U_{\mathrm{HH}}$, the wind speed from the WT1 nacelle-mounted anemometer $U_{\mathrm{nac},1}$, and $U_{\mathrm{REWS},1}$, derived from the power

https://doi.org/10.5194/wes-2026-93
Preprint. Discussion started: 29 June 2026


eawe european academy of wind energy
Open Access WIND ENERGY SCIENCE DISCUSSIONS

of WT1 as described in Schreiber et al. (2020a). The reference wind direction and turbulence intensity are taken from the met-mast sensors at hub height, while nacelle orientations are provided by SCADA data.

The results of this comparison are shown in Fig. 11a, which reports the normalized MAD between FLORIS predictions and the field-measured power. The numbers above the bars indicate percent changes relative to predictions based on met-mast measurements. A Pearson-correlation analysis (not shown for brevity) was carried out to detect discrepancies between the modeled and experimental power curves of each turbine; coefficients exceeded 0.95 for all wind-speed estimates considered. Predictions for the upstream turbine show substantial improvement when $U_{\mathrm{nac},1}$ is used as the reference wind speed, with a reduction in MAD of approximately 33% relative to the met-mast case. This improvement is likely due to the met-mast not being co-located with WT1. The best agreement between predicted and measured power is achieved when $U_{\mathrm{REWS},1}$ is used, which is expected since the REWS indirectly reflects the power produced by the upstream turbine. The figure further shows that the REWS also enhances predictions of the power of the downstream turbine. Overall, this analysis indicates that the REWS of WT1 provides the most accurate approximation of the cluster inflow wind speed, consistent with observations in Murphy et al. (2020). For this reason, this quantity is adopted as the FLORIS reference wind speed in the remainder of the paper.

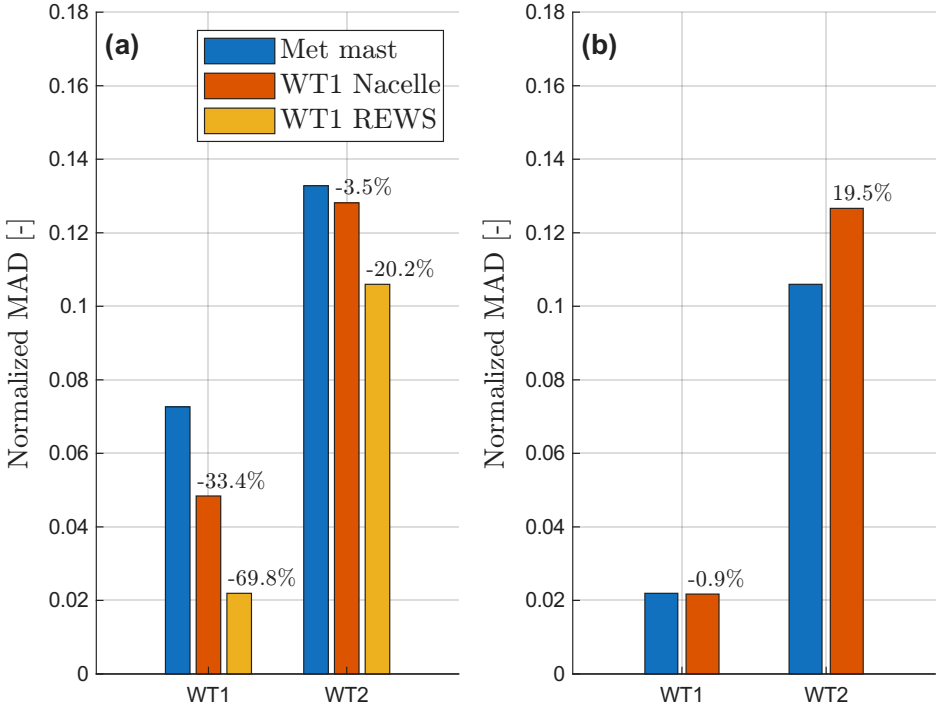


**Figure 11.** Normalized MAD between predicted and measured power for both turbines and different reference wind speed **(a)** and wind direction **(b)** estimations. The quantities above the bars indicate percent MAD variation with respect to the predictions performed with $U_{\mathrm{HH}}$ **(a)** or $\theta_{\mathrm{HH}}$ **(b)** as reference.

https://doi.org/10.5194/wes-2026-93
Preprint. Discussion started: 29 June 2026




Similarly, Fig. 11b compares FLORIS predictions based on two different estimates of the reference wind direction. The first is obtained from the wind vane on the met-mast at hub height ($\theta_{\mathrm{HH}}$), and the second from the sum of the nacelle position and the wind vane installed on the nacelle of WT1 ($\theta_{\mathrm{nac},1}$).

For the upstream turbine, both indicators yield very similar performance. Differences in the measured wind direction affect the simulated power of WT1 by altering its misalignment. The power of WT1 does not vary significantly as long as the misalignment remains small, which explains the similar MADs obtained from the two measurements. The situation differs for the downstream turbine, where FLORIS predictions of the relative wake position with respect to WT2 are highly sensitive to the wind direction. In this case, the met-mast provides more accurate estimates of the upstream wind direction. This is attributed to the frequent drifts and recalibrations of both yaw and nacelle-mounted wind-vane sensors, which are difficult to detect and correct (Simley et al., 2021; Fleming et al., 2014b). Moreover, the nacelle wind vane is affected by the wake generated by the upstream turbine itself (Mittelmeier and Kühn, 2018) and influenced by shear and veer (Howland et al., 2020; Hulsman et al., 2022), potentially introducing additional biases. For all these reasons, the met-mast is used as the reference wind-direction source in the remainder of the paper.

### 4.3 Comparison between baseline and Abkar veer models

The main objective of this section is to investigate whether model-plant mismatches can be reduced by using a wind-farm model that incorporates the effects of shear and veer presented in the previous sections. This is done by comparing mismatches between measured and simulated power of WT2.

Before comparing all models described in Sect. 3.4, it is useful to begin with a comparison of only the baseline and AV models. To examine the importance of including a veer-dependent wake skewing, model-plant mismatches on the downstream turbine are compared in Fig. 12, and are binned as functions of shear (panel a) and veer (panel b). Results are expressed in terms of normalized MAD, consistent with the previous section. The inputs for wind shear and veer are calculated from the met-mast. The uncertainty bands represent the 95% confidence interval of the MAD and are computed through bootstrapping.

It can be seen that, in the higher ranges of shear and veer, the AV model leads to improved performance in comparison to the baseline model. The improvement is more pronounced when examining errors as a function of wind veer, which is consistent with the fact that the AV model is specifically designed to predict a veer-induced wake skewing. The improvement observed as a function of wind shear follows from the correlation between shear and veer.

The results obtained so far indicate that a model capable of progressively skewing a wake under veering conditions provides a better match to the experimental results. The next section builds on these findings by comparing the remaining model variants described in Sect. 3.4.

### 4.4 Comparison of augmented models

The main goal of this section is to compare the remaining models listed in Table 2 to identify possible further reductions in model-plant mismatches.

https://doi.org/10.5194/wes-2026-93
Preprint. Discussion started: 29 June 2026


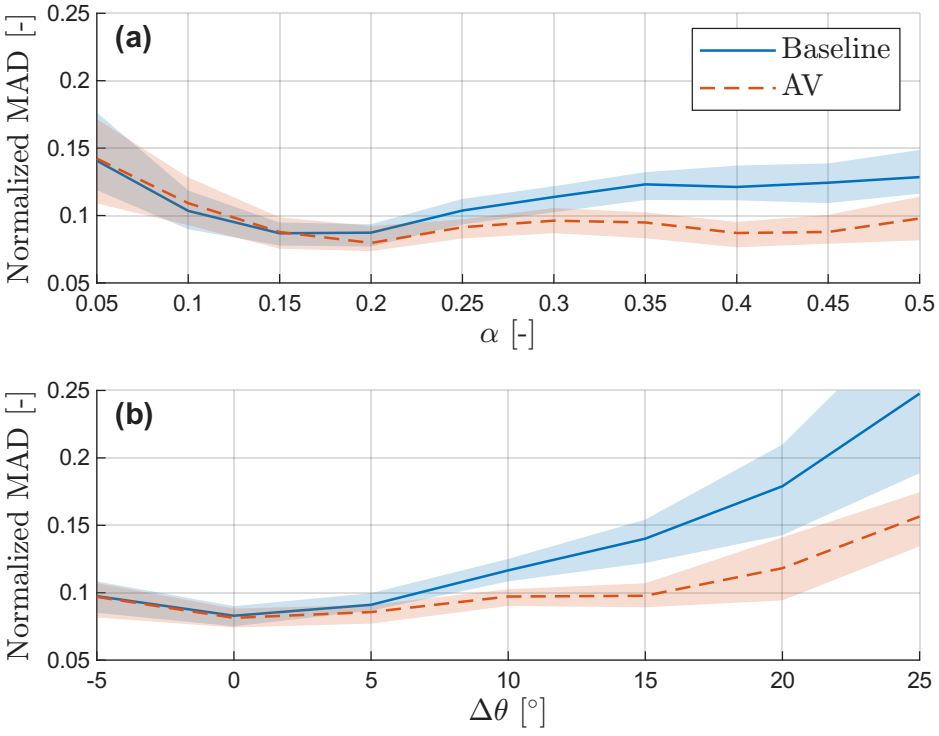


**Figure 12.** Normalized MAD and 95% confidence intervals (shaded areas) for the baseline wake model (solid blue line) and AV wake model (dashed red line), reported as functions of wind shear **(a)** and veer **(b)**.

The coefficients $M_1$ and $M_2$ of the $\mathrm{AV}_{\mathrm{augm}}$ model are tuned through the optimization framework described in Sect. 4.1. This leads to the following expressions for the term $a_d$ in Eq. (13):

$$a_d(\alpha_{\mathrm{mm}}) = (-0.36\,\alpha_{\mathrm{mm}} + 0.064)D, \tag{16a}$$

$$a_d(\alpha_{\mathrm{obs}}) = (-0.31\,\alpha_{\mathrm{mm}} + 0.035)D. \tag{16b}$$

Results are shown in Fig. 13. In addition to the AV model, the figure includes the augmented $\mathrm{AV}_{\mathrm{augm}}$ model, which incorporates the shear-dependent wake displacement of Eq. (16). The other models included are $\mathrm{AV}_{\mathrm{augm},\Delta\theta(\alpha_{\mathrm{mm}})}$ and $\mathrm{AV}_{\mathrm{augm},\Delta\theta(\alpha_{\mathrm{obs}})}$, which differ only in the technique used for wind-shear estimation. The latter approach represents a configuration that does not require a met-mast installation, and therefore is the only practically usable one in a realistic controls application.

Results are expressed as differences between the normalized MAD and the corresponding value of the baseline model, to highlight differences among the models and to offset the influence of an inflow-dependent model-plant mismatch (which can still be observed in Fig. 12).

The first observation is that $\mathrm{AV}_{\mathrm{augm}}$ generally performs better than all other models. Given the dependency between shear and wake displacement already discussed, this increase in accuracy is expected. The improvement is more pronounced for moderate-to-high wind shears, which is the range specifically targeted by the model. Another reason for the superior accuracy

https://doi.org/10.5194/wes-2026-93
Preprint. Discussion started: 29 June 2026


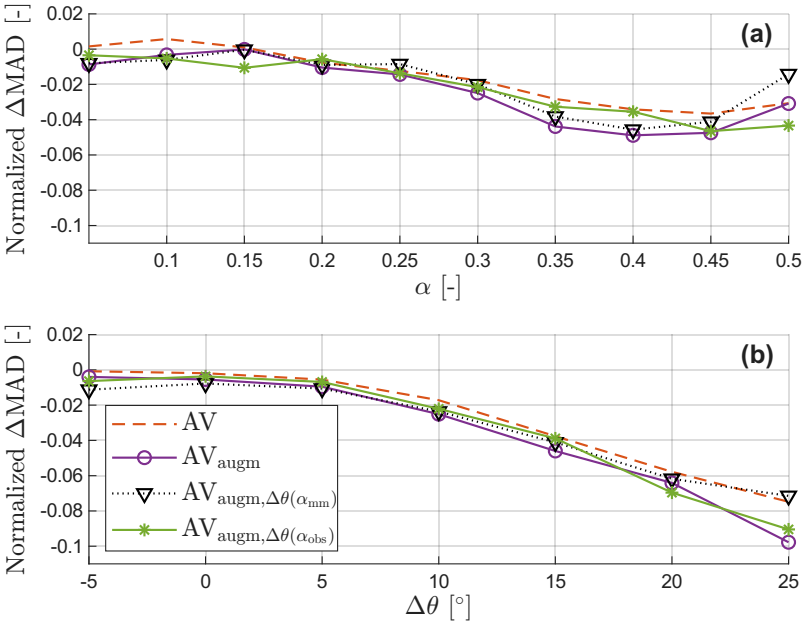


**Figure 13.** Comparison among the different wake models errors, expressed with respect to the baseline model as $\Delta\mathrm{MAD} = \mathrm{MAD}_{\mathrm{model}} - \mathrm{MAD}_{\mathrm{baseline}}$, and normalized using WT2 median power. Results are plotted as functions of wind shear **(a)**, and wind veer **(b)**.

of $\mathrm{AV}_{\mathrm{augm}}$ is that both $\mathrm{AV}_{\mathrm{augm},\Delta\theta(\alpha_{\mathrm{mm}})}$ and $\mathrm{AV}_{\mathrm{augm},\Delta\theta(\alpha_{\mathrm{obs}})}$ are simplified variants of this model and require only four inflow inputs instead of five.

For low shears and low veers, all models provide very similar results, leading to nearly overlapping curves. These conditions are typically associated with higher turbulence intensities, which result in higher MAD for all models (these results are omitted here for brevity, but are shown in Fig. 12).

Another noteworthy point is that the $\mathrm{AV}_{\mathrm{augm},\Delta\theta(\alpha_{\mathrm{mm}})}$ model yields consistent improvements with respect to the baseline model and even outperforms the AV model, except for very high shear values. This indicates that, for the site under consideration, the relationship between shear and veer can be exploited to reduce the required equipment, without significant losses in predictive accuracy. However, this relationship may depend on the site and on the wind direction, and therefore an accurate assessment of wind gradients remains necessary.

As mentioned at the beginning of the paper, measuring either wind shear or wind veer poses a challenge and cannot be achieved using the standard equipment installed on wind turbines. Typically, instruments such as LiDARs or met-masts are required, increasing cost and complexity. In the case of met-masts, the lack of co-location with wind turbines presents additional difficulties, especially for large wind farms. An alternative is provided by wind-sensing technologies that rely on on-board sensors to determine the wind characteristics impinging on the rotor.

This solution is represented by the $\mathrm{AV}_{\mathrm{augm},\Delta\theta(\alpha_{\mathrm{obs}})}$ model. From the figure, it can be seen that the wind estimator provides a viable alternative to a met-mast. More specifically, for medium-low wind shears ($0.1 < \alpha < 0.2$), the use of the wind estimator

https://doi.org/10.5194/wes-2026-93
Preprint. Discussion started: 29 June 2026


eawe european academy of wind energy
Open Access WIND ENERGY SCIENCE DISCUSSIONS

slightly improves predictions. This finding may indicate that lower shears (often associated with higher turbulence intensities) are better captured by the wind estimator than by the met-mast, possibly because of the rotor-effective nature of the estimator.

For very high wind shears ($\alpha > 0.45$), the wind estimator also performs better than the met-mast, while in the medium range ($0.2 < \alpha < 0.3$) no noticeable differences appear. In the range of high shear ($0.32 < \alpha < 0.42$), the met-mast performs better than the observer. When mismatches are binned by wind veer, both the mast and the observer behave similarly for low to moderate veers, after which errors naturally increase due to the simplified interpolation $\Delta\theta(\alpha)$. It is worth noting that, for higher wind veers, the wind estimator performs better than the met-mast, which may again be due to the fact that a rotor-effective shear correlates better with a rotor-effective wind veer.

Overall, the results indicate that the "rotor as a sensor" wind estimator can improve accuracy with respect to both the baseline and the AV wake model. For the test site under consideration, a wind estimator can provide a wind-shear input during operation without significant loss of accuracy in comparison to a nearby met-mast measurement.

### 4.5 Considerations on wake steering strategies

The purpose of this section is to discuss the impact of the wake models presented in Sects. 4.3 and 4.4 on wake-steering strategies. A key limitation of the present analysis is that it was not possible to evaluate the real-world effects of each strategy in the field. Therefore, all conclusions are based exclusively on optimal offset angles and simulated power differences among the models.

For each model considered, optimal LUTs are calculated using the robust approach described by Simley et al. (2020), which maximizes the expected power production under wind-direction and yaw-position uncertainties:

$$\gamma^*(\hat{\boldsymbol{x}}) = \arg\max_{\gamma} E[P(\hat{\boldsymbol{x}}, \gamma)], \tag{17}$$

where $\hat{\boldsymbol{x}}$ represents the inflow variables of the optimization, and $E[\cdot]$ indicates the expected value. The optimization is performed for three of the models analyzed in Sect. 4.4: the baseline model, the $\mathrm{AV}_{\mathrm{augm}}$ model, and the $\mathrm{AV}_{\mathrm{augm},\Delta\theta(\alpha_{\mathrm{obs}})}$ model. This selection enables a comparison among the baseline condition, a model that includes the effects of both wind shear and veer (with five inflow inputs), and a model that relies solely on rotor-observed shear.

The vector $\hat{\boldsymbol{x}}$ depends on the wake model: $\hat{\boldsymbol{x}} = \theta, U, \alpha, \mathrm{TI}, \Delta\theta$ for the baseline and $\mathrm{AV}_{\mathrm{augm}}$ models, and $\hat{\boldsymbol{x}} = \theta, U, \alpha, \mathrm{TI}$ for the $\mathrm{AV}_{\mathrm{augm},\Delta\theta(\alpha_{\mathrm{obs}})}$ model. Details on the implementation can be found in Simley et al. (2020) and are omitted here for brevity. The uncertainties are kept at their original values, namely 4.95° and 1.75° for wind-direction and yaw-misalignment, respectively.

The resulting LUTs are shown in Figs. 14a and 14b for two wind-shear values, illustrating the differences induced by the various modeling approaches. As expected, for the baseline model the switching point at which the optimal offset changes sign remains constant, whereas it shifts for the other models.

Percentage power gains relative to greedy operation are evaluated for each optimal LUT using the same dataset used in Sect. 4.3. Results are calculated for wind-direction bins of 2° and are shown in Fig. 14c (low $\alpha$) and Fig. 14d (high $\alpha$). For

https://doi.org/10.5194/wes-2026-93
Preprint. Discussion started: 29 June 2026




eawe european academy of wind energy
Open Access WIND ENERGY SCIENCE DISCUSSIONS

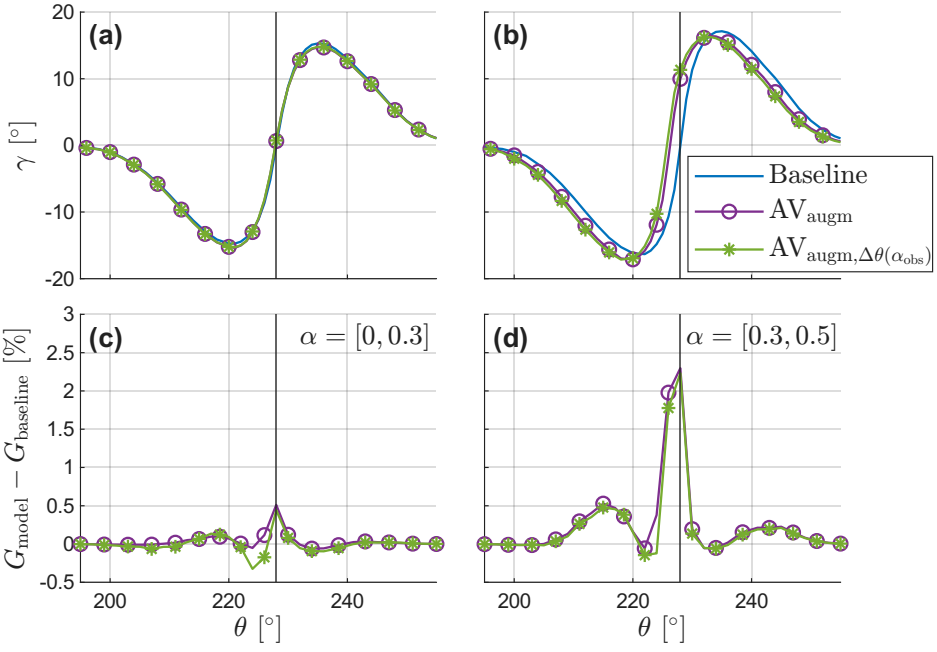


**Figure 14.** Optimized wind turbine misalignment for the different models, for $U = 8$ ms$^{-1}$, TI $= 10\%$, and $\Delta\theta = 5°$, for the shear values $\alpha = 0.1$ **(a)** and $\alpha = 0.3$ **(b)**. A vertical line is drawn at 228.0°, corresponding to the wind direction for which the two wind turbines are aligned. Increase in power gains with respect to the baseline model, shown as a function of inflow wind direction for low **(c)** and high **(d)** wind shear.

clarity, only the difference between the power gain of each augmented model, $G_{\text{model}}$, and the baseline power gain, $G_{\text{baseline}}$, is reported.

It is important to highlight that the performance of the LUTs is evaluated using the FLORIS model equipped with the $\text{AV}_{\text{augm}}$ model. Since the calculation of the baseline LUT does not account for the effects of shear and veer, lower power gains are expected for this model than for the other ones. This is confirmed by the results, as the augmented models consistently outperform the baseline. The comparison underscores the effect of "wrong-way steering" caused by inaccurate ambient-condition modeling, which in this case leads to approximately 2% lower gains in the region of full wake overlap.

Notably, $\text{AV}_{\text{augm}}$ and $\text{AV}_{\text{augm},\Delta\theta(\alpha_{\text{obs}})}$ yield essentially identical results, although the former requires five inflow parameters instead of four. In practice, this means that the additional on-site infrastructure required for such measurements could be avoided by relying on a "rotor as a sensor" wind estimator. Wind-sensing strategies that exploit the relationship between wind shear and veer may therefore offer performance improvements while requiring only limited supplementary investment (null, when blade loads are already installed for other reasons).

Overall, the results indicate that, at least from a theoretical perspective, wake-steering strategies may increase energy capture when the underlying wake model correctly accounts for the influence of wind shear and veer. The observed gain is primarily associated with the avoidance of steering in an incorrect direction, an effect likely to become even more relevant in wind farms

https://doi.org/10.5194/wes-2026-93
Preprint. Discussion started: 29 June 2026




with larger turbine spacing than the very short distance of the present setup. Potential implications for structural loads should also be considered.

As noted earlier, the main limitation of the present analysis is that the LUTs have not been tested in the field. As a result, these findings should be regarded as qualitative rather than quantitative, and further experimental validation is required.

## 5 Conclusions

In this paper, experimental results from a two-turbine cluster were analysed with the goal of investigating the influence of wind shear and veer on the power loss of the downstream turbine. This was enabled by the particularly stable atmospheric conditions at the site, which resulted in a wide range of shear and veer values. Even for non-misaligned turbines, it was shown that an increase in either wind shear or veer causes a displacement of the wake toward the right when looking downstream. For wind veer, this observed displacement is only apparent and arises from the different hub heights of the two turbines, because the physical effect of veer is to skew the wake rather than to laterally shift it.

To validate and isolate the effect of shear, LES simulations were conducted. These simulations corroborated the experimental findings by showing similar trends in wake displacement, although with smaller magnitudes than those observed in the field. The physical mechanism responsible for shear-induced wake displacement is not yet fully understood and has been attributed in the literature to the advection of low-velocity wake regions into higher-velocity flow due to wake rotation, as well as interactions between the wake and the ground. In the present study, by using a BEM-based model, it is shown that wake displacement is consistent with a residual lateral force acting on the rotor as a function of wind shear. This explanation is considered sufficient for the scope of this work, although further investigations are needed to fully understand the interplay between residual forces and wake development.

Different methods for estimating inflow inputs to an engineering wake model were investigated. The analysis shows that a rotor-effective wind speed is the most reliable indicator of the inflow wind speed, and that the met-mast provides the most accurate indicator of the inflow wind direction. However, the met-mast is adequate for the present small test site as it is close to the turbines, but it may become insufficient for larger wind farms, where alternative methodologies – such as consensus-based (Annoni et al., 2019) or wind-farm-scale flow estimators – may be required.

It was shown that wind veer should be accounted for within engineering wake models. Its effect is to progressively skew the wake as it moves downstream, and incorporating this effect leads to improved accuracy in power predictions. In addition, a shear-dependent displacement of the wake toward the right was identified, and incorporating this phenomenon into the wake model further reduced model-plant mismatch.

The challenge posed by the lack of inflow-gradient measurements in standard wind-turbine instrumentation was also discussed. Wind-sensing techniques were shown to be suitable candidates for estimating vertical shear, thereby enabling the inclusion of these potentially important effects within wake-steering strategies. Wind sensing can also estimate veer (Bertelè et al., 2024), although this capability was not considered here. The analysis further showed that, for the present test site, the

https://doi.org/10.5194/wes-2026-93
Preprint. Discussion started: 29 June 2026




correlation between wind shear and wind veer can be exploited to reduce the number of inflow inputs required by a wind-farm model while still reducing model-plant mismatch relative to the baseline model.

Optimal LUTs for power maximization were generated for several of the wake models considered. The results show that neglecting the impact of shear and veer on the wake can lead to wrong-way steering in the region close to full wake overlap, thereby reducing the effectiveness of wake-steering strategies. However, since it was not possible to validate the optimal LUTs in the field, these findings remain theoretical and require further experimental confirmation.

Finally, the analysis presented here relies exclusively on non-misaligned operating conditions in the free-field experiments. As a result, the conclusions may differ when yaw offsets are considered in a full-scale setup.

## Appendix A: Wind characteristics

The discussion regarding the relationship between wind shear and veer in Sect. 2.2 is here complemented by presenting histograms of both quantities. The distributions of shear and veer for south-westerly winds recorded during the campaign are shown in Fig. A1, together with their median values. As already noted in the paper, a broad range of atmospheric conditions occurred during the experiment, including relatively high wind-shear values. The distribution of wind veer is positively skewed, which is consistent with expectations given the location of the test site.

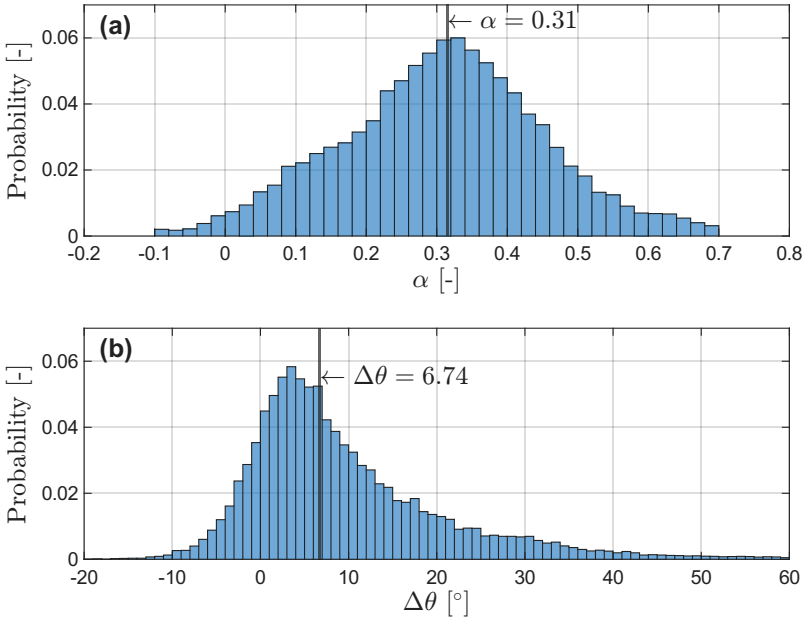


**Figure A1.** Frequency distributions of the met-mast measurements: vertical shears **(a)** and wind veers **(b)**. Vertical lines correspond to median values.

https://doi.org/10.5194/wes-2026-93
Preprint. Discussion started: 29 June 2026


To further characterize the relationship between veer and shear, the distributions shown in Fig. A1 were categorized according to bins of increasing wind-shear values. This analysis reveals the dependency of wind veer on shear at the site (Fig. A2). For increasing wind shears, the corresponding median values of $\Delta\theta$ tend to increase, which is compatible with more stable atmospheric conditions for those wind regimes. Moreover, as wind shear increases (that is, for more stable stratification), the positive tail of the veer distribution becomes longer, indicating a wider range of possible veering conditions.

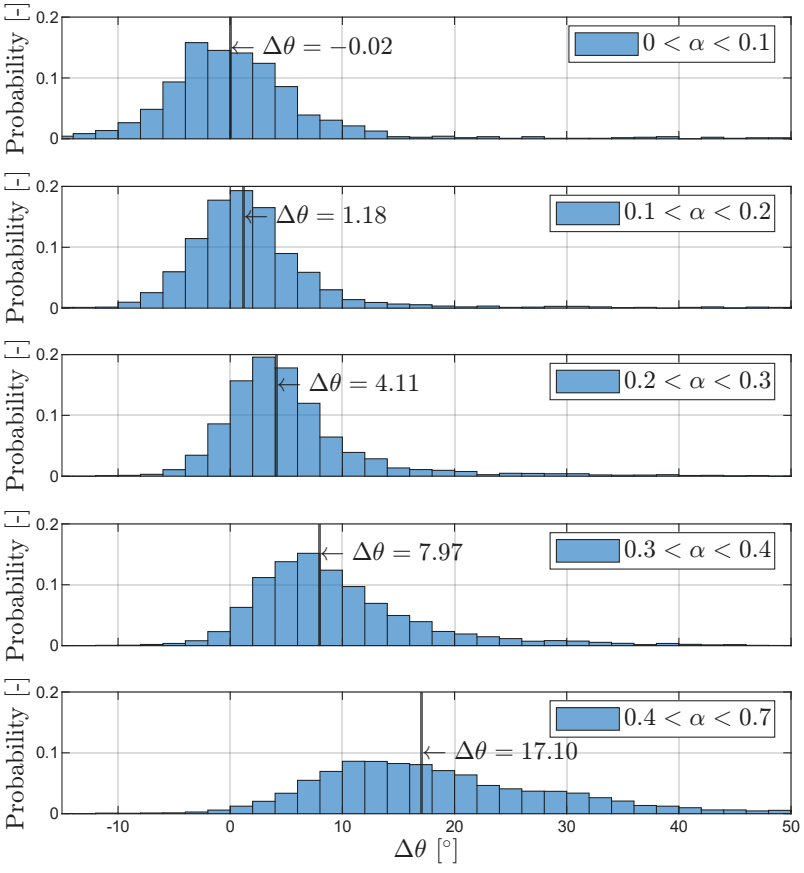


**Figure A2.** Frequency distribution of wind veers, binned for increasing wind shears.

## Appendix B: Wake stretching

For the AV model, the wake deficit of Eq. (9a) becomes:

$$\frac{u(x,y,z)}{U_\infty} = 1 - C(x)e^{-((y+x\tan(\Delta\theta/D(z-z_{\mathrm{HH}}))-\Delta y_{\mathrm{wc}})^2/2\sigma_y^2+(z-z_{\mathrm{HH}})^2/2\sigma_z^2)}. \tag{B1}$$

https://doi.org/10.5194/wes-2026-93
Preprint. Discussion started: 29 June 2026


eawe european academy of wind energy
Open Access WIND ENERGY SCIENCE DISCUSSIONS

By applying a small-angle approximation and neglecting $z_{\mathrm{HH}}$ and $\Delta y_{\mathrm{wc}}$, the parameters $\ell_y$, $\ell_{yz}$, and $\ell_z$ that govern the shape of the ellipses can be obtained by comparing Eq. (9a) and Eq. (B1). This yields:

$$\ell_y = \frac{1}{2\sigma_y^2}, \tag{B2a}$$

$$\ell_{yz} = -\frac{x\Delta\theta/D}{2\sigma_y^2}, \tag{B2b}$$

$$\ell_z = \left((x\Delta\theta/D)^2 \frac{\sigma_z^2}{\sigma_y^2} + 1\right) \frac{1}{2\sigma_z^2}. \tag{B2c}$$

It is instructive to compare the semi-axes of the original Gaussian model (equal to $\sigma_y$ and $\sigma_z$) with those of the AV model, in order to quantify the "stretching" of the wake as a function of the incoming wind veer for the test site under consideration. The lengths of the major and minor semi-axes are given by:

$$\sigma_{\mathrm{AV}y}^2 = \frac{1}{2(\ell_y \cos^2\psi + 2\ell_{yz}\cos\psi\sin\psi + \ell_z \sin^2\psi)}, \tag{B3a}$$

$$\sigma_{\mathrm{AV}z}^2 = \frac{1}{2(\ell_z \cos^2\psi - 2\ell_{yz}\cos\psi\sin\psi + \ell_y \sin^2\psi)}, \tag{B3b}$$

with:

$$\psi = \frac{1}{2}\arctan\left(\frac{2\ell_{yz}}{\ell_y - \ell_z}\right). \tag{B4}$$

This comparison is performed for varying wind-veer values for the test site under investigation. Results are shown in Fig. B1 and are consistent with the findings of Sect. 4.3: for low wind veer, the behaviour of the models is very similar, whereas the difference in wake shape increases with increasing veer.

## Appendix C: Nomenclature and abbreviations

| | |
|---|---|
| $A$ | Rotor disk area |
| $a_0$ | Axial induction factor (0P, constant over the rotor disk) |
| $a_d$ | Gaussian model wake deflection: initial offset |
| $b_d$ | Gaussian model wake deflection: slope coefficient |
| $C$ | Maximum velocity deficit in Gaussian wake model |
| $C_D$ | Drag coefficient |
| $C_{L,\alpha}$ | Slope of the lift coefficient |
| $C_S$ | Lateral force coefficient |
| $C_T$ | Thrust coefficient |
| $D$ | Rotor diameter |
| $G_{\mathrm{model}}$ | Model power gain |
| $G_{\mathrm{baseline}}$ | Baseline power gain |

https://doi.org/10.5194/wes-2026-93
Preprint. Discussion started: 29 June 2026


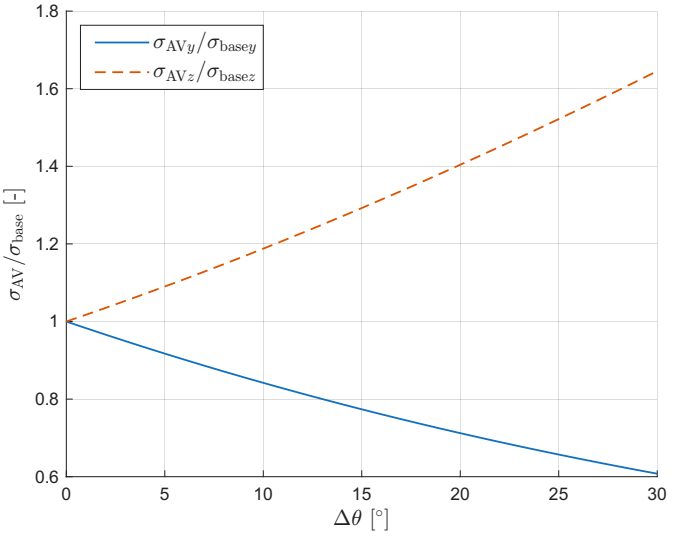


**Figure B1.** Ratio between the major and minor semi-axes of the AV model and the baseline model, calculated for the test site under consideration and for different wind veers.

| | |
|---|---|
| $k$ | Vertical shear linear coefficient |
| $K_{a,b}$ | Coefficients defining relationship between turbulence intensity and width of the Gaussian wake |
| $\ell_y$ | Baseline model coefficient defining the lateral wake expansion |
| $\ell_{yz}$ | Baseline model coefficient defining the coupling between lateral and vertical wake expansion |
| $\ell_z$ | Baseline model coefficient defining the vertical wake expansion |
| $M_1$ | Wake displacement coefficient proportional to shear |
| $M_2$ | Wake displacement constant coefficient |
| $N_{\mathrm{gauss},\alpha}$ | Gaussian model parameter linking turbulence intensity to far-wake onset |
| $N_{\mathrm{gauss},\beta}$ | Gaussian model parameter linking induction factor to far-wake onset |
| $p_p$ | Exponent of the cosine power law |
| $P_1$ | Power output of upstream turbines |
| $P_2$ | Power output of downstream turbines |
| $P_{\mathrm{greedy}}$ | Power output of the baseline (“greedy”) case |
| $P_{\mathrm{wfc}}$ | Power output of the wake-steering controlled case |
| $q$ | Dynamic pressure |
| $r_{1\text{-}2}$ | Distance between upstream and downstream turbines |
| $S$ | Lateral force, positive when pointing to the right looking downstream |
| $u$ | Local longitudinal wind speed in the wake |
| $U$ | Wind speed |

https://doi.org/10.5194/wes-2026-93
Preprint. Discussion started: 29 June 2026


eawe european academy of wind energy
Open Access WIND ENERGY SCIENCE DISCUSSIONS

| | | |
|---|---|---|
| | $U_\infty$ | Undisturbed wind speed |
| | $U_{\mathrm{HH}}$ | Wind speed measured at hub height by the met-mast |
| | $U_{\mathrm{nac},1}$ | Wind speed measured by the nacelle-mounted anemometer of WT1 |
| | $U_{\mathrm{REWS},1}$ | Rotor-effective wind speed of WT1 |
| | $U_{\mathrm{REWS},2}$ | Rotor-effective wind speed of the virtual downstream turbine |
| | $x$ | Downstream coordinate in the wind-farm reference frame |
| | $x'$ | Dummy integration variable |
| | $y$ | Lateral (cross-stream) coordinate in the wind-farm reference frame |
| | $z$ | Vertical coordinate in the wind-farm reference frame |
| | | |
| | $\alpha$ | Wind shear exponent |
| | $\alpha_{\mathrm{mm}}$ | Wind shear exponent measured by the met-mast |
| | $\alpha_{\mathrm{obs}}$ | Wind shear exponent estimated by the wind observer |
| | $\beta$ | Blade pitch angle |
| | $\gamma$ | Yaw misalignment angle |
| | $\gamma^*$ | Optimal yaw misalignment |
| | $\Delta E$ | Increase in total energy production relative to the greedy case |
| | $\Delta y_{\mathrm{wc}}$ | Wake centerline lateral displacement |
| | $\Delta\theta$ | Wind veer across the entire rotor |
| | $\theta$ | Wind direction |
| | $\theta_{1\text{-}2}$ | Relative wind direction between WT1 and WT2 |
| | $\theta_{\mathrm{HH}}$ | Wind direction measured at hub height by the met-mast |
| | $\theta_{\mathrm{nac},1}$ | Wind direction estimated from WT1 nacelle sensors |
| | $\theta_{\mathrm{wc,fit}}$ | Fitted wake centerline wind direction |
| | $\lambda$ | Tip-speed ratio |
| | $\xi$ | Linear wake expansion coefficient |
| | $\rho$ | Air density |
| | $\sigma_y$ | Standard deviation defining wake width in the lateral direction |
| | $\sigma_z$ | Standard deviation defining wake width in the vertical direction |
| | $\chi$ | Skew angle of the wake |
| | $\chi_0$ | Initial skew angle |
| | $\psi$ | Rotation angle of the Gaussian wake ellipse |
| | | |
| | $\hat{\boldsymbol{x}}$ | Vector of inflow variables used in the optimization process |

https://doi.org/10.5194/wes-2026-93
Preprint. Discussion started: 29 June 2026


eawe european academy of wind energy
Open Access WIND ENERGY SCIENCE DISCUSSIONS

| | |
|---|---|
| ABL | Atmospheric boundary layer |
| AV | Abkar veer model |
| $\mathrm{AV}_{\mathrm{augm}}$ | Augmented Abkar veer model |
| $\mathrm{AV}_{\mathrm{augm},\Delta\theta(\alpha_{\mathrm{mm}})}$ | Augmented Abkar veer model with veer correlated to met-mast shear |
| $\mathrm{AV}_{\mathrm{augm},\Delta\theta(\alpha_{\mathrm{obs}})}$ | Augmented Abkar veer model with veer correlated to wind-observer shear |
| BEM | Blade element momentum |
| CFD | Computational fluid dynamics |
| FLORIS | FLOw Redirection and Induction in Steady State |
| GPS | Global positioning system |
| HH | Hub height |
| IEC | International Electrotechnical Commission |
| IEA | International Energy Agency |
| LCOE | Levelized cost of energy |
| LES | Large eddy simulation |
| LB | Lower blade |
| LiDAR | Light detection and ranging |
| LUT | Look-up table |
| MAD | Median absolute deviation |
| MM | Met-mast or meteorological mast |
| NN | Neural network |
| NREL | National Renewable Energy Laboratory |
| REWS | Rotor-effective wind speed |
| RMSE | Root mean square error |
| SOWFA | Simulator for Wind Farm Applications |
| SVD | Singular value decomposition |
| TI | Turbulence intensity |
| TUM | Technical University of Munich |
| UTM | Universal transverse mercator |
| WT1 | Upstream wind turbine |
| WT2 | Downstream wind turbine |

https://doi.org/10.5194/wes-2026-93
Preprint. Discussion started: 29 June 2026


eawe european academy of wind energy
Open Access WIND ENERGY SCIENCE DISCUSSIONS

*Code and data availability.* The operational data and turbine model used in this research are property of eno energy systems GmbH. All figures and the data used to generate them can be retrieved in Pickle Python and MATLAB formats via https://doi.org/10.5281/zenodo.19484474 (Sucameli et al., 2026).

*Author contributions.* CRS conducted the main research work, built the experimental dataset, post-processed and analyzed the results in collaboration with FC, and wrote a first draft of the manuscript in close collaboration with CLB. CLB developed the concept and model of wake deflection caused by a shear-induced lateral force, suggested the use of the rotor-as-a-sensor to provide inputs to the shear and veer-aware models, and supervised the research. MB developed and validated the wind estimator, and supported its integration within the experimental dataset. RB supported the tuning of FLORIS wake model. ST conducted the LES simulations. PH contributed to the conduction of the experimental campaign. All authors provided important input to this research work through discussions and feedback and by writing the paper.

*Competing interests.* At least one of the (co-)authors is a member of the editorial board of *Wind Energy Science*.

*Acknowledgements.* The authors express their gratitude to eno energy systems GmbH, for granting access to their turbines, and to Alexander Gerds, for providing continuous support during the measurement campaign. The authors also thank Johannes Schreiber for many fruitful discussions.

*Financial support.* This work has been supported by the CompactWind II project (FKZ: 0325492G), which receives funding from the German Federal Ministry for Economic Affairs and Climate Action (BMWK). Additional funding was provided by the European Union under the Horizon Europe grant No. 101084216 (project MERIDIONAL).

https://doi.org/10.5194/wes-2026-93
Preprint. Discussion started: 29 June 2026


eawe european academy of wind energy
Open Access WIND ENERGY SCIENCE DISCUSSIONS

## References

Abkar, M. and Porté-Agel, F.: Influence of atmospheric stability on wind-turbine wakes: A large-eddy simulation study, Physics of Fluids, 27, 035 104, https://doi.org/10.1063/1.4913695, 2015.

Abkar, M., Sørensen, J. N., and Porté-Agel, F.: An Analytical Model for the Effect of Vertical Wind Veer on Wind Turbine Wakes, Energies, 11, https://doi.org/10.3390/en11071838, 2018.

Annoni, J., Fleming, P., Scholbrock, A., Roadman, J., Dana, S., Adcock, C., Porte-Agel, F., Raach, S., Haizmann, F., and Schlipf, D.: Analysis of control-oriented wake modeling tools using lidar field results, Wind Energy Science, 3, 819–831, https://doi.org/10.5194/wes-3-819-2018, 2018.

Annoni, J., Bay, C., Johnson, K., Dall'Anese, E., Quon, E., Kemper, T., and Fleming, P.: Wind direction estimation using SCADA data with consensus-based optimization, Wind Energy Science, 4, 355–368, https://doi.org/10.5194/wes-4-355-2019, 2019.

Bastankhah, M. and Porté-Agel, F.: A new analytical model for wind-turbine wakes, Renewable Energy, 70, 116–123, https://doi.org/https://doi.org/10.1016/j .renene.2014.01.002, special issue on aerodynamics of offshore wind energy systems and wakes, 2014.

Bastankhah, M. and Porté-Agel, F.: Experimental and theoretical study of wind turbine wakes in yawed conditions, Journal of Fluid Mechanics, 806, 506–541, https://doi.org/10.1017/jfm.2016.595, 2016.

Becker, M., Ritter, B., Doekemeijer, B., van der Hoek, D., Konigorski, U., Allaerts, D., and van Wingerden, J.-W.: The revised FLORIDyn model: implementation of heterogeneous flow and the Gaussian wake, Wind Energy Science, 7, 2163–2179, https://doi.org/10.5194/wes-7-2163-2022, 2022.

Bertelè, M., Bottasso, C. L., and Schreiber, J.: Wind inflow observation from load harmonics: initial steps towards a field validation, Wind Energy Science, 6, 759–775, https://doi.org/10.5194/wes-6-759-2021, 2021.

Bertelè, M., Meyer, P. J., Sucameli, C. R., Fricke, J., Wegner, A., Gottschall, J., and Bottasso, C. L.: The rotor as a sensor – observing shear and veer from the operational data of a large wind turbine, Wind Energy Science, 9, 1419–1429, https://doi.org/10.5194/wes-9-1419-2024, 2024.

Bertelè, M. and Bottasso, C.: Initial results from the field testing of the "rotor as a sensor" concept, Journal of Physics: Conference Series, 1452, 012 074, https://doi.org/10.1088/1742-6596/1452/1/012074, 2020.

Blondel, F. and Cathelain, M.: An alternative form of the super-Gaussian wind turbine wake model, Wind Energy Science, 5, 1225–1236, https://doi.org/10.5194/wes-5-1225-2020, 2020.

Bodini, N., Zardi, D., and Lundquist, J. K.: Three-dimensional structure of wind turbine wakes as measured by scanning lidar, Atmospheric Measurement Techniques, 10, 2881–2896, https://doi.org/10.5194/amt-10-2881-2017, 2017.

Bortolotti, P., Tarrés, H., Dykes, K., Merz, K., Sethuraman, L., Verelst, D., and Zahle, F.: IEA Wind TCP Task 37: Systems Engineering in Wind Energy-WP2.1 Reference Wind Turbines, National Renewable Energy Laboratory (NREL), https://doi.org/10.2172/1529216, 2019.

Bottasso, C. and Riboldi, C.: Estimation of wind misalignment and vertical shear from blade loads, Renewable Energy, 62, 293–302, https://doi.org/https://doi.org/10.1016/j .renene.2013.07.021, 2014.

Bottasso, C. L., Cacciola, S., and Iriarte, X.: Calibration of wind turbine lifting line models from rotor loads, Journal of Wind Engineering and Industrial Aerodynamics, 124, 29–45, https://doi.org/https://doi.org/10.1016/j.jweia.2013.11.003, 2014.

Braunbehrens, R., Vad, A., and Bottasso, C. L.: The wind farm as a sensor: learning and explaining orographic and plant-induced flow heterogeneities from operational data, Wind Energy Science Discussions, 2022, 1–50, https://doi.org/10.5194/wes-2022-67, 2022.

https://doi.org/10.5194/wes-2026-93
Preprint. Discussion started: 29 June 2026


Braunbehrens, R., Vad, A., and Bottasso, C. L.: The wind farm as a sensor: learning and explaining orographic and plant-induced flow heterogeneities from operational data, Wind Energy Science, 8, 691–723, https://doi.org/10.5194/wes-8-691-2023, 2023.

Bromm, M., Vollmer, L., and Kühn, M.: Numerical investigation of wind turbine wake development in directionally sheared inflow, Wind Energy, 20, 381–395, https://doi.org/https://doi.org/10.1002/we.2010, 2017.

Bulaevskaya, V., Wharton, S., Clifton, A., Qualley, G., and Miller, W. O.: Wind power curve modeling in complex terrain using statistical models, Journal of Renewable and Sustainable Energy, 7, 013 103, https://doi.org/10.1063/1.4904430, 2015.

Churchfield, M. and Sirnivas, S.: On the Effects of Wind Turbine Wake Skew Caused by Wind Veer, Tech. rep., National Renewable Energy Lab. (NREL), Golden, CO (United States), https://doi.org/10.2514/6.2018-0755, 2018.

Doekemeijer, B. M., Kern, S., Maturu, S., Kanev, S., Salbert, B., Schreiber, J., Campagnolo, F., Bottasso, C. L., Schuler, S., Wilts, F., Neumann, T., Potenza, G., Calabretta, F., Fioretti, F., and van Wingerden, J.-W.: Field experiment for open-loop yaw-based wake steering at a commercial onshore wind farm in Italy, Wind Energy Science, 6, 159–176, https://doi.org/10.5194/wes-6-159-2021, 2021.

Englberger, A. and Lundquist, J. K.: How does inflow veer affect the veer of a wind-turbine wake?, Journal of Physics: Conference Series, 1452, 012 068, https://doi.org/10.1088/1742-6596/1452/1/012068, 2020.

Englberger, A., Lundquist, J. K., and Dörnbrack, A.: Changing the rotational direction of a wind turbine under veering inflow: a parameter study, Wind Energy Science, 5, 1623–1644, https://doi.org/10.5194/wes-5-1623-2020, 2020.

Fleming, P., Annoni, J., Shah, J. J., Wang, L., Ananthan, S., Zhang, Z., Hutchings, K., Wang, P., Chen, W., and Chen, L.: Field test of wake steering at an offshore wind farm, Wind Energy Science, 2, 229–239, https://doi.org/10.5194/wes-2-229-2017, 2017.

Fleming, P., King, J., Dykes, K., Simley, E., Roadman, J., Scholbrock, A., Murphy, P., Lundquist, J. K., Moriarty, P., Fleming, K., van Dam, J., Bay, C., Mudafort, R., Lopez, H., Skopek, J., Scott, M., Ryan, B., Guernsey, C., and Brake, D.: Initial results from a field campaign of wake steering applied at a commercial wind farm – Part 1, Wind Energy Science, 4, 273–285, https://doi.org/10.5194/wes-4-273-2019, 2019.

Fleming, P., King, J., Simley, E., Roadman, J., Scholbrock, A., Murphy, P., Lundquist, J. K., Moriarty, P., Fleming, K., van Dam, J., Bay, C., Mudafort, R., Jager, D., Skopek, J., Scott, M., Ryan, B., Guernsey, C., and Brake, D.: Continued results from a field campaign of wake steering applied at a commercial wind farm – Part 2, Wind Energy Science, 5, 945–958, https://doi.org/10.5194/wes-5-945-2020, 2020.

Fleming, P. A., Gebraad, P. M., Lee, S., van Wingerden, J.-W., Johnson, K., Churchfield, M., Michalakes, J., Spalart, P., and Moriarty, P.: Evaluating techniques for redirecting turbine wakes using SOWFA, Renewable Energy, 70, 211–218, https://doi.org/https://doi.org/10.1016/j.renene.2014.02.015, special issue on aerodynamics of offshore wind energy systems and wakes, 2014a.

Fleming, P. A., Scholbrock, A. K., Jehu, A., Davoust, S., Osler, E., Wright, A. D., and Clifton, A.: Field-test results using a nacelle-mounted lidar for improving wind turbine power capture by reducing yaw misalignment, Journal of Physics: Conference Series, 524, 012 002, https://doi.org/10.1088/1742-6596/524/1/012002, 2014b.

FLORIS: FLORIS: FLOw Redirection and Induction in Steady State, https://github.com/NatLabRockies/floris, last accessed 29 January 2026, 2025.

Gao, L., Li, B., and Hong, J.: Effect of wind veer on wind turbine power generation, Physics of Fluids, 33, 015 101, https://doi.org/10.1063/5.0033826, 2021.

Gao, L., Milliren, C., Dasari, T., Knoll, A. A., and Hong, J.: Catch the wind: Optimizing wind turbine power generation by addressing wind veer effects, PNAS Nexus, 3, pgae480, https://doi.org/10.1093/pnasnexus/pgae480, 2024.

Gebraad, P. M. O., Churchfield, M. J., and Fleming, P. A.: Incorporating Atmospheric Stability Effects into the FLORIS Engineering Model of Wakes in Wind Farms, Journal of Physics: Conference Series, 753, 052 004, https://doi.org/10.1088/1742-6596/753/5/052004, 2016a.

https://doi.org/10.5194/wes-2026-93
Preprint. Discussion started: 29 June 2026


Gebraad, P. M. O., Teeuwisse, F. W., van Wingerden, J. W., Fleming, P. A., Ruben, S. D., Marden, J. R., and Pao, L. Y.: Wind plant power optimization through yaw control using a parametric model for wake effects—a CFD simulation study, Wind Energy, 19, 95–114, https://doi.org/https://doi.org/10.1002/we.1822, 2016b.

Gomez, M. S. and Lundquist, J. K.: The Effects of Wind Veer During the Morning and Evening Transitions, Journal of Physics: Conference Series, 1452, 012 075, https://doi.org/10.1088/1742-6596/1452/1/012075, 2020.

Greenshields, C.: OpenFOAM v6 User Guide, The OpenFOAM Foundation, London, UK, https://doc.cfd.direct/openfoam/user-guide-v6, 2018.

Holton, J. R.: An introduction to dynamic meteorology, International Geophysics Series, Elsevier Academic Press,, Burlington, MA, 4 edn., ISBN 9780123540157, http://books.google.com/books?id=fhW5oDv3EPsC, 2004.

Howland, M. F., Lele, S. K., and Dabiri, J. O.: Wind farm power optimization through wake steering, Proceedings of the National Academy of Sciences, 116, 14 495–14 500, 2019.

Howland, M. F., González, C. M., Martínez, J. J. P., Quesada, J. B., Larrañaga, F. P., Yadav, N. K., Chawla, J. S., and Dabiri, J. O.: Influence of atmospheric conditions on the power production of utility-scale wind turbines in yaw misalignment, Journal of Renewable and Sustainable Energy, 12, 063 307, https://doi.org/10.1063/5.0023746, 2020.

Hulsman, P., Sucameli, C., Petrović, V., Rott, A., Gerds, A., and Kühn, M.: Turbine power loss during yaw-misaligned free field tests at different atmospheric conditions, Journal of Physics: Conference Series, 2265, 032 074, https://doi.org/10.1088/1742-6596/2265/3/032074, 2022.

Jiménez, A., Crespo, A., and Migoya, E.: Application of a LES technique to characterize the wake deflection of a wind turbine in yaw, Wind Energy, 13, 559–572, https://doi.org/https://doi.org/10.1002/we.380, 2010.

Jonkman, J. and Shaler, K.: FAST.Farm user's guide and theory manual, 2021.

Kim, K.-H., Bertelè, M., and Bottasso, C. L.: Wind inflow observation from load harmonics via neural networks: A simulation and field study, Renewable Energy, 204, 300–312, https://doi.org/https://doi.org/10.1016/j .renene.2022.12.051, 2023.

Kuhn, M., Henry de Frahan, M., Mohan, P., Deskos, G., Churchfield, M., Cheung, L., Sharma, A., Almgren, A., Ananthan, S., Brazell, M., Martínez-Tossas, L., Thedin, R., Rood, J., Sakievich, P., Vijayakumar, G., Zhang, W., and Sprague, M.: AMR-Wind: A Performance-Portable, High-Fidelity Flow Solver for Wind Farm Simulations, Wind Energy, 28, e70 010, https://doi.org/https://doi.org/10.1002/we.70010, e70010 we.70010, 2025.

Ma, X., Poulsen, N., and Bindner, H.: Estimation of Wind Speed in Connection to a Wind Turbine, Informatics and Mathematical Modelling, Technical University of Denmark, DTU, 1995.

Martínez-Tossas, L. A., Annoni, J., Fleming, P. A., and Churchfield, M. J.: The aerodynamics of the curled wake: a simplified model in view of flow control, Wind Energy Science, 4, 127–138, https://doi.org/10.5194/wes-4-127-2019, 2019.

Martínez-Tossas, L. A., King, J., Quon, E., Bay, C. J., Mudafort, R., Hamilton, N., Howland, M. F., and Fleming, P. A.: The curled wake model: a three-dimensional and extremely fast steady-state wake solver for wind plant flows, Wind Energy Science, 6, 555–570, https://doi.org/10.5194/wes-6-555-2021, 2021.

Meyers, J., Bottasso, C., Dykes, K., Fleming, P., Gebraad, P., Giebel, G., Göçmen, T., and van Wingerden, J.-W.: Wind farm flow control: prospects and challenges, Wind Energy Science, 7, 2271–2306, https://doi.org/10.5194/wes-7-2271-2022, 2022.

Mittelmeier, N. and Kühn, M.: Determination of optimal wind turbine alignment into the wind and detection of alignment changes with SCADA data, Wind Energy Science, 3, 395–408, https://doi.org/10.5194/wes-3-395-2018, 2018.

https://doi.org/10.5194/wes-2026-93
Preprint. Discussion started: 29 June 2026


Mohammadi, M., Bastankhah, M., Fleming, P., Churchfield, M., Bossanyi, E., Landberg, L., and Ruisi, R.: Curled-Skewed Wakes behind Yawed Wind Turbines Subject to Veered Inflow, Energies, 15, https://doi.org/10.3390/en15239135, 2022.

Murphy, P., Lundquist, J. K., and Fleming, P.: How wind speed shear and directional veer affect the power production of a megawatt-scale operational wind turbine, Wind Energy Science, 5, 1169–1190, https://doi.org/10.5194/wes-5-1169-2020, 2020.

Niayifar, A. and Porté-Agel, F.: Analytical Modeling of Wind Farms: A New Approach for Power Prediction, Energies, 9, https://doi.org/10.3390/en9090741, 2016.

Rott, A., Doekemeijer, B., Seifert, J. K., van Wingerden, J.-W., and Kühn, M.: Robust active wake control in consideration of wind direction variability and uncertainty, Wind Energy Science, 3, 869–882, https://doi.org/10.5194/wes-3-869-2018, 2018.

Sagaut, P.: Large Eddy Simulation for Incompressible Flows: An Introduction, Scientific Computation, Springer, Berlin, https://doi.org/10.1007/b137536, 2006.

Sanchez Gomez, M. and Lundquist, J. K.: The effect of wind direction shear on turbine performance in a wind farm in central Iowa, Wind Energy Science, 5, 125–139, https://doi.org/10.5194/wes-5-125-2020, 2020.

Schottler, J., Mühle, F., Bartl, J., Peinke, J., Adaramola, M. S., Sætran, L., and Hölling, M.: Comparative study on the wake deflection behind yawed wind turbine models, Journal of Physics: Conference Series, 854, 012 032, https://doi.org/10.1088/1742-6596/854/1/012032, 2017.

Schreiber, J., Bottasso, C., and Bertelè, M.: Field testing of a local wind inflow estimator and wake detector, Wind Energy Science, 5, 867–884, https://doi.org/10.5194/wes-5-867-2020, 2020a.

Schreiber, J., Bottasso, C. L., Salbert, B., and Campagnolo, F.: Improving wind farm flow models by learning from operational data, Wind Energy Science, 5, 647–673, https://doi.org/10.5194/wes-5-647-2020, 2020b.

Shu, Z., Li, Q., He, Y., and Chan, P. W.: Investigation of Marine Wind Veer Characteristics Using Wind Lidar Measurements, Atmosphere, 11, https://doi.org/10.3390/atmos11111178, 2020.

Simley, E., Fleming, P., and King, J.: Design and analysis of a wake steering controller with wind direction variability, Wind Energy Science, 5, 451–468, https://doi.org/10.5194/wes-5-451-2020, 2020.

Simley, E., Fleming, P., Girard, N., Alloin, L., Godefroy, E., and Duc, T.: Results from a wake-steering experiment at a commercial wind plant: investigating the wind speed dependence of wake-steering performance, Wind Energy Science, 6, 1427–1453, https://doi.org/10.5194/wes-6-1427-2021, 2021.

Stoevesandt, B., Schepers, G., Fuglsang, P., and Yuping, S.: Handbook of Wind Energy Aerodynamics, Springer Nature, 2022, ISBN 978-3-030-05455-7, https://doi.org/10.1007/978-3-030-05455-7, 2020.

Sucameli, C. R., Bertelè, M., Braunbehrens, R., Campagnolo, F., Tamaro, S., Hulsman, P., and Bottasso, C. L.: Figures for the paper: On the effects of wind shear and veer on the power of a downstream turbine, https://doi.org/10.5281/zenodo.19484475, 2026.

Tamaro, S., Campagnolo, F., and Bottasso, C. L.: On the power and control of a misaligned rotor – beyond the cosine law, Wind Energy Science, 9, 1547–1575, https://doi.org/10.5194/wes-9-1547-2024, 2024.

TurbSim(2023): https://github.com/old-NWTC/TurbSim, turbSim, last access: 01 August 2023.

Vanderwende, B. J. and Lundquist, J. K.: The modification of wind turbine performance by statistically distinct atmospheric regimes, Environmental Research Letters, 7, 034 035, https://doi.org/10.1088/1748-9326/7/3/034035, 2012.

Vollmer, L., Steinfeld, G., Heinemann, D., and Kühn, M.: Estimating the wake deflection downstream of a wind turbine in different atmospheric stabilities: an LES study, Wind Energy Science, 1, 129–141, https://doi.org/10.5194/wes-1-129-2016, 2016.

Wang, J., Wang, C., Campagnolo, F., and Bottasso, C. L.: Wake behavior and control: comparison of LES simulations and wind tunnel measurements, Wind Energy Science, 4, 71–88, https://doi.org/10.5194/wes-4-71-2019, 2019.

https://doi.org/10.5194/wes-2026-93
Preprint. Discussion started: 29 June 2026


Wharton, S. and Lundquist, J. K.: Atmospheric stability affects wind turbine power collection, Environmental Research Letters, 7, 014 005, https://doi.org/10.1088/1748-9326/7/1/014005, 2012.

Wiser, R. H., Rand, J., Seel, J., Beiter, P., Baker, E., Lantz, E., and Gilman, P.: Expert elicitation survey predicts 37% to 49% declines in wind energy costs by 2050, Nature Energy, https://doi.org/https://dx.doi.org/10.1038/s41560-021-00810-z, 2021.